Volume 19, Number 3

September, 1965

SOVIET ATOMIC ENERGY

АТОМНАЯ ЭНЕРГИЯ
(ATOMNAYA ÉNERGIYA)

TRANSLATED FROM RUSSIAN

CONSULTANTS BUREAU

SOVIET ATOMIC ENERGY

A translation of **ATOMNAYA ÉNERGIYA,**
a publication of the Academy of Sciences of the USSR

Volume 19, Number 3 September, 1965

CONTENTS

Annual Subscription: $95 **Single Issue: $30** **Single Article: $15**

COLLECTIVE INTERACTION OF "RUNAWAY" ELECTRONS WITH PLASMA IN THE S-1 STELLARATOR

(UDC 533.2)

P. I. Blinov and L. P. Zakatov

Translated from Atomnaya Énergiya, Vol. 19, No. 3, pp. 233-238, September, 1965
Original article submitted November 18, 1964

The authors study the interaction of "runaway" electrons with plasma during the ohmic loading time of the S-1 Stellarator, and the associated radio emission.

As is well-known, when an electric field is applied to a plasma there arises a current of runaway electrons. For all the electrons to become runaway, the field must, as shown in [1], exceed a certain critical value

$$E_{\text{crit}} \approx e/\lambda_D^2,$$

where λ_D is the Debye radius. If the field is weak, only those electrons with velocities well above thermal will enter the runaway state, i.e., a state of unlimited acceleration. In race-track type apparatus, runaway electrons must quite quickly emerge from the plasma, exciting bremsstrahlung x-rays from the beam-limiting diaphragms and chamber walls in the region of curvature.

On the other hand, a directed electron current in a plasma can excite electrostatic oscillations [2, 3]. For this to occur, as shown in [2], the directed velocity of the electron current must exceed the thermal velocity of the plasma electrons. Thus the growth of electrostatic oscillations prevents unlimited acceleration of the electrons in the plasma.

The oscillations take several of their own periods to develop [4]. Meanwhile the runaway electrons are rapidly retarded to near thermal velocities, causing an abrupt decrease of the current in the plasma. If the electric field is not switched off, the process of acceleration and retardation will be repeated periodically.

When scattered at inhomogeneities in the plasma and at the plasma-vacuum boundaries, longitudinal vibrations can be transformed into transverse ones and be radiated out of the plasma [5, 6]. This effect is caused by interactions between the harmonics of the electrostatic oscillations [7]. Thus the presence of x-ray and radio emission from the Stellarator during the ohmic loading period may indicate the presence in the plasma of runaway electrons. The appearance of runaway electrons in a Stellarator was first observed in [8]. Collective interaction of runaway electrons with plasma in strong electric fields was studied in detail in [9, 10].

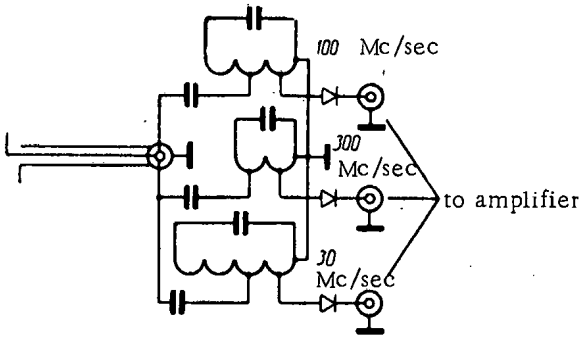

Fig. 1. Receiving circuit for 30-300 Mc/sec range.

EXPERIMENTAL METHOD

The construction of the S-1 Stellarator is described in [11]. The initial pressure in the chamber was $2 \cdot 10^{-7}$ mm Hg. All the measurements were made on helium in the pressure range $1.1 \cdot 10^{-4}$ to $2 \cdot 10^{-3}$ mm Hg.

Radio emission from the plasma was studied over a wide frequency range, from tens of kc/sec to tens of gigacycles/sec. Low-frequency noise (down to tens of kc/sec) was received by magnetic or dipole antennae placed near the straight part of the chamber, and after amplification was fed to the input of an OK-24 oscillograph. Radiation in the range 30-2000 Mc/sec was received similarly and led via a coaxial cable to a selective circuit (Fig. 1). To avoid re-

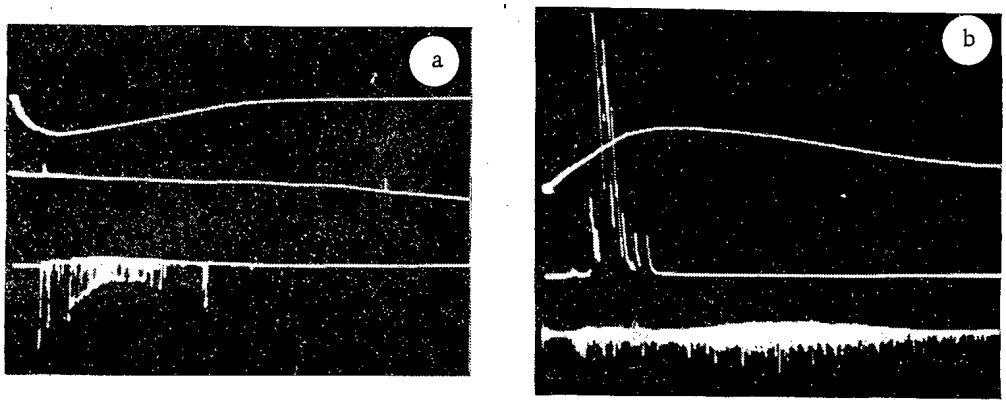

Fig. 3. Oscillograms of current, radiofrequency emission (λ = 3 cm) and x-ray emission from plasma (top downwards, respectively). a) Electric field antiparallel to retaining magnetic field (sweep time 6 msec, attenuation at oscillograph input 1 : 1 for radio waves, 1 : 500 for x-rays); b) electric field parallel to magnetic field (sweep time 3 msec, attenuation at oscillograph input 1 : 5 for radio waves, 1 : 1 for x-rays).

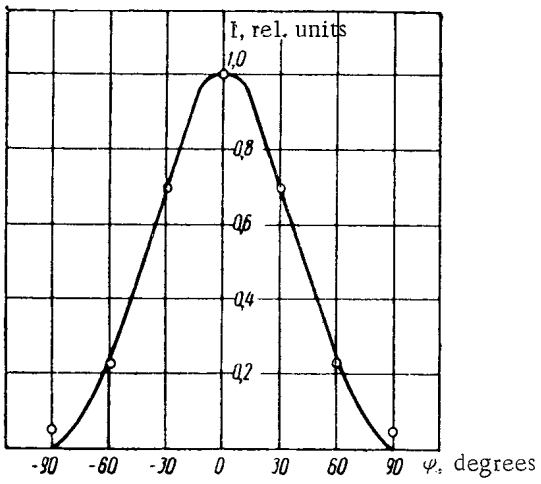

Fig. 4. Detector current versus angle of rotation antenna. ○) Experimental points; ——) theoretical curve.

For a pinch of diameter 8 cm, $N_{run} \approx 10^9$ cm^{-3}, i.e., $N_{run} \approx 10^{-3}$ N, since the mean electron concentration N at the moment of appearance of radio emission is below 10^{12} cm^{-3}.

A current jump of 100 amp with accelerating voltage 300 V over the entire length of the race-track corresponds to a power of 30 kw expended on slowing down the electrons. According to [12], about half of this power (in our case about 15 kw) is expended on swinging the electrostatic vibrations. The experimentally measured radiative power at 3 cm wavelength was 25 mw/cm^2 with field frequency 60 Mc/sec, i.e., seven orders of magnitude higher than the power of thermal radiation for electrons at a temperature of 100 eV. If we assume that the radiation is uniformly distributed along the whole length of the chamber, the full radiative power for the same frequency band is 400 watts, corresponding to about 3% of the power of the electrostatic vibrations as calculated in [12].

Reduction in N_{run}/N (e.g., by escape of runaway electrons from the beam) must lead to reduction in level or even collapse of the electrostatic vibrations. On the other hand, such losses must be accompanied by intense x-radiation from the chamber walls. Measurements showed that changes in the direction of the electric field in relation to the magnetic field lead to abrupt changes in the amounts of x-ray and radio emission. The intensity of x-ray emission was a maximum with the electric field E antiparallel to the magnetic field H, whereas in this case the radio emission was relatively weak. When the direction of E was reversed, the power of the radio emission rose sharply, while the intensity of x-ray emission fell by a factor of about 100 (Fig. 3). This may indicate that, in the first case, hydromagnetic instability was occurring: in the S-1 Stellarator the angle through which the lines of magnetic force curve at the boundary of the plasma pinch is nearly -2π, and therefore in the first case the Kruskal-Shafranov limit is reached at lower plasma currents than in the second case.

POLARIZATION

The polarization of the radiation was measured in the three-centimeter region. The dielectric antenna was connected via a rectangular waveguide to a detector head against which was placed a low-quality resonator, which was designed to separate a relatively narrow frequency spectrum. The transmission band of the resonator was 50 Mc at 9650 Mc. By rotating the whole channel around the axis of the antenna, it was possible to measure how the radio-emission intensity varied with the angle between the plane of polarization of the waveguide and the axis of the vacu-

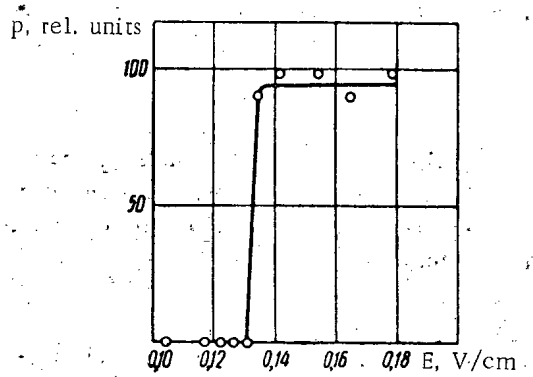

Fig. 7. Radio power emitted, versus electric field intensity.

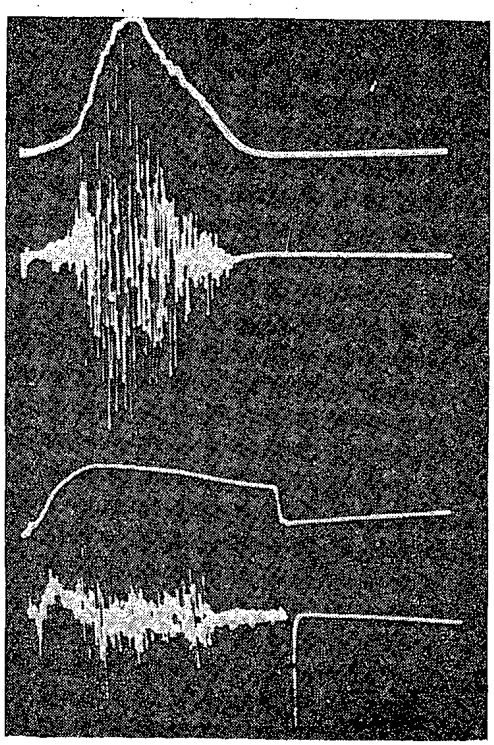

Fig. 9. Oscillograms of current and low-frequency signal from magnetic probe, for various discharge conditions.

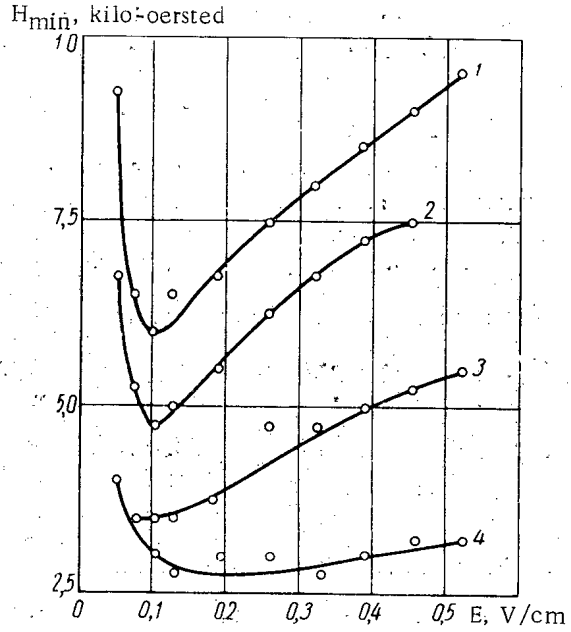

Fig. 8. H_{min}, field for beginning of radio emission, versus applied electric field E, for various chamber pressures, mm Hg: 1) $1.1 \cdot 10^{-4}$; 2) $1.7 \cdot 10^{-4}$; 3) $2.5 \cdot 10^{-4}$; 4) $4 \cdot 10^{-3}$.

Figure 6 plots E_{min} versus the initial pressure in the chamber: the graph is nearly linear. This relation follows from Dreicer's theory [1]: the deviation from a straight line shows that the temperature and degree of ionization of the plasma vary with the pressure.

Let us compare E_{min} with the value predicted by the Dreicer formula:

$$E_{crit} = 1.5 \cdot 10^{-8} \frac{N}{T_e}, \text{V/cm},$$

where T_e is the electron temperature in °K. Radiation with wavelength 3 cm corresponds to a density of order 10^{12} cm^{-3}, and the electron temperature is then about 30 eV for initial pressure 10^{-4} mm Hg. Then E_{crit} = 0.05 V/cm, which is about 2.5 times greater than the experimental value, E_{min} = 0.02 V/cm. This fact, together with the stepwise graph of radiative power versus E (Fig. 7), shows that electrostatic vibrations arise only when a significant fraction of the electrons enter the runaway state.

At pressures above $1.5 \cdot 10^{-3}$ mm Hg, the radiation vanishes at all frequencies. This is apparently due to increased damping of the vibrations.

Relation between Emission and Magnetic Field Intensity

It has been noted that radiation from the plasma is observed only when the magnetic field exceeds a certain value. At lower fields there is no radiation. The minimum field intensity was found to depend on the bypass voltage (i.e., on the electric field intensity E), and also on the initial chamber pressure and the size of the diaphragm limiting the diameter of the plasma pinch.

As seen from Fig. 8, with increasing bypass voltage, H_{min} at first falls sharply, then passes through a minimum and begins to increase slowly. As the pressure increases the critical magnetical fields decrease. However, the value of E corresponding to the minimum of the critical magnetic field is practically independent of the initial pressure.

STABILITY OF A PARTIALLY COMPENSATED ELECTRON BEAM

(UDC 533.9)

B. V. Chirikov

Translated from Atomnaya Énergiya, Vol. 19, No. 3,
pp. 239-244, September, 1965
Original article submitted August 13, 1964; in revised form, April 12, 1965

The author discusses the conditions for stability of a partially compensated electron beam in relation to deflection ("snaking"). It is shown that, with a continuous spectrum of perturbation wave vectors, there is always a region of strong instability (with relatively large increments). With a discrete spectrum (e.g., with a beam of finite length in an accelerator), instability occurs only at beam currents greater than a certain critical value. Landau damping and radiation friction do not eliminate the instability. A weak dissipative instability is discovered, caused by radiation friction. In some cases Landau damping stabilizes this instability, but can also increase it.

The investigation is based on a model beam in the form of two pinches, electron and ion, with constant dimensions and uniform densities.

Studies of the stability of a particle beam in an accelerator are usually limited to the single-particle approximations, i.e., they discuss the motion of a single particle in the external fields. In this case the stability problem can practically be solved unambigously and reduces to a suitable choice of external fields.* To a first approximation, the interaction between particles can be regarded as the electrostatic repulsion, and hence we can estimate the limiting current. In actual fact, partly or wholly compensated beams in an accelerator form an unusual kind of plasma. It is well-known that in a plasma ther can be a number of instabilities due to the interactions of a large number of charged particles. The question arises: How far can these instabilities arise in accelerators? This problem was first dealt with by Budker [3] for a so-called stabilized electron beam. One of the most deleterious plasma instabilities was found to be beam deflection ("snaking"). In [3] is was shown that polarization of the beam, i.e., relative displacement of electrons and ions, eliminates this instability for sufficiently shortwave initial perturbations; it was suggested that long-wave perturbations might also be stabilized by external fields. This type of instability was further discussed in [4, 5]. The authors concluded that full stability can only be attained in a strong-focusing external magnetic field, and not by eddy currents or weak focusing. These results were obtained by treating separately stabilization by the external field and by polarization, the assumption being made that, to get stabilization, it is enough for these two stability regions to overlap. This treatment is in general incorrect, because new effects may arise from the simultaneous action of both forces. In this paper it will be shown that the simultaneous action of polarization and external forces always leads to instability for a certain range of wavelengths.

1. Dispersion Equation

Following [3-5], we shall begin by examining the stability of the simplest model: the electrons and ions are regarded as forming two cylindrical pinches of the same radius a, with constant densities n_e and n_i, for which we shall use the dimensionless values

$$\nu_e = \frac{\pi a^2 e^2 n_e}{mc^2}; \quad \nu_i = \frac{\pi a^2 e^2 n_i}{mc^2}, \tag{1}$$

* However, in systems with no damping (e.g., in proton storage rings), it is possible for delicate nonlinear effects to arise, of the stochastic-instability [1] or separatrix-splitting [2] type: these are difficult to calculate.

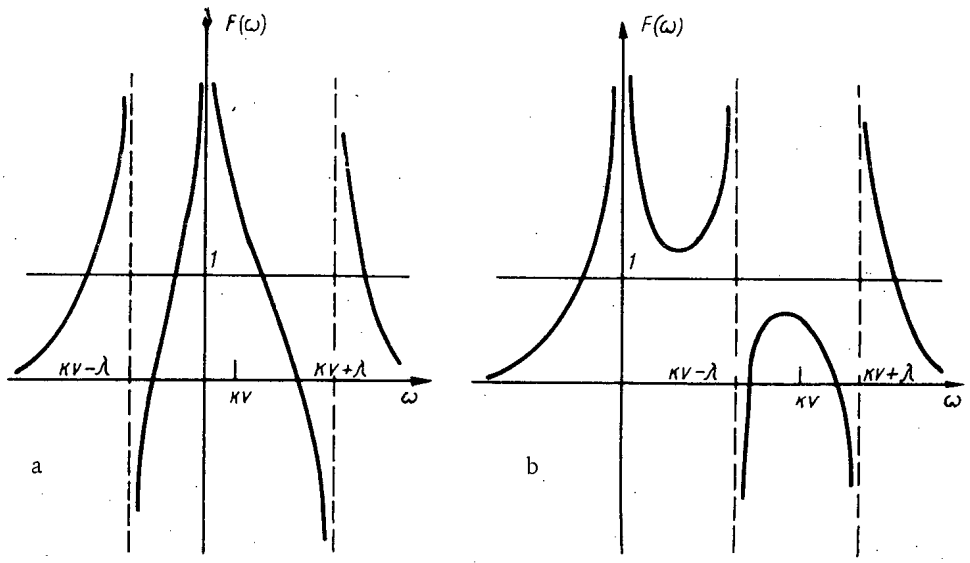

Frequency dependence of $F(\omega)$. a) $kv < \lambda$ (stability); b) $kv > \lambda$ (instability).

3. Zones of Instability and Increments

Let us first consider the case $\xi << 1$, which is the case with relatively small compensation, $\alpha >> \gamma m/M << 1$. As remarked above, the zone of instability is then $(\lambda/v) < k < k_2$, since the maximum of $F(\omega)$ is less than zero for all $k > (\lambda/v)$. Calculating k_2, we find the region of instability to be

$$\lambda^2 < (kv)^2 < \lambda^2 + \Omega^2 \left[1 + 3\xi^{1/3} \left(1 + \frac{\lambda^2}{\Omega^2} \right)^{1/3} \right], \tag{8}$$

which becomes smaller but does not vanish when $\Omega < \lambda$, corresponding to overlapping of the regions of stabilization by polarization and by the external field.

The complex roots in the instability zone are

$$\omega \approx \xi \frac{kv\Omega^4}{[\Omega^2 + \lambda^2 - (kv)^2]^2} \pm i \sqrt{\xi\Omega^2 \frac{(kv)^2 - \lambda^2}{\Omega^2 + \lambda^2 - (kv)^2}}. \tag{9}$$

Hence it is seen that the increment is relatively small ($\sim \sqrt{\xi}$) and the instability is almost aperiodic ($\mathrm{Re}\omega << \mathrm{Im}\omega$). The most unfavorable part of the zone of instability is its right hand edge, $(kv)^2 \to \Omega^2 + \lambda^2$. In this case the approximate expression (9) is inapplicable and must be replaced by

$$\omega \approx \Omega \left(\frac{\xi\Omega}{4\sqrt{\Omega^2 + \lambda^2}} \right)^{1/3} (1 \pm i). \tag{10}$$

In practice, however, the maximum increment can be determined from the frequency scatter $\Delta\Omega$.* To make an exact allowance for these fluctuations, we must abandon our simple model. We can make a rough estimate of their effect if we assume that the minimum difference

$$\Omega^2 + \lambda^2 - (kv)^2 = 2\Omega^2\delta, \text{where } \delta = \frac{\Delta\Omega}{\Omega}.$$

From Eq. (9) we get

* It is important that there is a continuous frequency spectrum, i.e., a spectrum of random fluctuations of frequency Ω, which is just so for a beam which is usually located in a highly nonequilibrium state. On the contrary, a spatial and slowly changing inhomogeneity of the external fields leads only to displacement of the frequency λ and does not impose limits on ω. Exceptions to this are external forces caused by eddy currents, since these fluctuate proportionally to the beam current.

$$\nu_e < \frac{\gamma\beta^2}{2\alpha}\left(\frac{a}{R}\right)^2\left(\frac{Q}{16\xi}\right)^{1/3}. \tag{17}$$

This value, though less than Eq. (16) [($\xi >> 1$)], is still very large, owing to the smallness of $\alpha << (\gamma m/M)$.

5. Frictional Forces

Let us consider the effect of friction. By this we mean any force directed against the electron velocity. Remembering that $y_e \sim \exp i\,(kx - \omega t)$, we can write ($\lambda_1 > 0$)

$$f_T = -\gamma m\lambda_1 \dot{y}_e = -i\,(kv - \omega)\,\lambda_1 y_e \gamma m. \tag{18}$$

The frictional force is equivalent to an imaginary term added to the external force:

$$\lambda^2 \longrightarrow \lambda^2 + i\lambda_1\,(kv - \omega). \tag{19}$$

Assuming that this added term is sufficiently small ($\lambda_1 \to 0$), we can find a correction $\Delta\omega$ in the formula

$$\frac{\partial F\,(\omega,\,\lambda^2)}{\partial\lambda^2}\,\Delta\lambda^2 + \frac{\partial F\,(\omega,\,\lambda^2)}{\partial\omega}\,\Delta\omega + \frac{\partial^2 F\,(\omega,\,\lambda^2)}{\partial\omega^2}\cdot\frac{(\Delta\omega)^2}{2} = 0, \tag{20}$$

where $\Delta\lambda^2 = i\lambda_1\,(kv - \omega)$, and for ω we are substituting the roots of the dispersion Eq. (7).

Let us consider the expression for the correction to the frequency in the linear approximation (20):

$$\Delta\omega = -i\lambda_1\,(kv - \omega)\,\frac{\partial F/\partial\lambda^2}{\partial F/\partial\omega}. \tag{21}$$

Since $\frac{\partial F}{\partial\lambda^2} = \frac{\Omega^2}{[(kv-\omega)^2 - \lambda^2]^2} > 0$, the sign of $\mathrm{Im}(\Delta\omega)$ is determined by the signs of $kv - \omega$ and $\partial F/\partial\omega$ and can be either negative (damping) or positive (instability). Since $\mathrm{Im}(\Delta\omega) \sim (\partial F/\partial\omega)^{-1}$, it is clear that the strongest effect of friction corresponds exactly to the maximum and minimum of $F(\omega)$. In this case, by Eq. (20),

$$\Delta\omega = \pm\sqrt{-i\lambda_1\,(kv - \omega)\,\frac{\partial F/d\lambda^2}{\partial^2 F/d\omega^2}}. \tag{22}$$

Radiation friction, which is most important for electrons, is unfortunately too weak to suppress the type of instability under consideration. However, appreciable instability may arise under the action of frictional forces.

The physical significance of this dissipative instability is that the velocity of the electrons ($\dot{y} \sim kv - \omega$) may be directed in a sense contrary to the local wave velocity [$(\partial y/\partial t) \sim -\omega$]. Then the frictional force coincides in direction with the wave velocity and may lead to oscillation. The mechanism of the oscillation is associated with scattering of electrons in the field of the ion pinch, which vibrates with a certain phase difference from the electron pinch. Hence, it is clear that dissipative instability based on frictional forces is possible only in the presence of ions.

6. Landau Damping

Let us now consider the scatter of the longitudinal velocities of electrons and ions,* which is known to cause damping of the vibrations [7]. We shall confine ourselves to the discussion of a simplified dispersion equation [8]. This equation can be derived from the expression for the polarization force Eq. (2), in which y_e and y_i must be replaced by the electron and ion displacements averaged over the distribution function. This calculation yields

$$\xi\Omega^2\int\frac{f_i\,du}{(\omega - ku)^2} + \Omega^2\int\frac{f_e\,dv}{(\omega - kv)^2 - \lambda^2} = 1. \tag{23}$$

The exact theory [7] shows that the integration in Eq. (23) must be carried out in the complex plane of the variables v, u, bypassing the zero denominators (v_0, u_0) by a circuit from below. The ionic and electronic Landau damping are

* We regard the ions as nonmagnetic.

$\omega \approx kv \pm \lambda$, as the velocity distribution of the electrons is usually fairly narrow. The physical meaning of the instability is the same as that discussed in Section 5, as in the ultimate analysis Landau damping is due to particle collisions, i.e., it is a special kind of friction. The importance of the collisions follows from the assumption [7] that the distribution function is constant. The part played by collisions was demonstrated clearly in [9, 10]. Instability due to Landau damping is evidently similar in its mechanism to the so-called universal instability in a plasma [11].

We take this opportunity to thank G. I. Budker, V. M. Galitskii, V. I. Karpman, S. S. Moiseev, R. Z. Sagdeev, V. V. Sokolov, A. M. Stefanovskii, and I. B. Khriplovich for helpful discussions.

LITERATURE CITED

1. B. V. Chirikov, Atomnaya Énergiya, 6, 630 (1959).
2. V. K. Mel'nikov, Dokl. AN SSSR, 148, 1259 (1963).
3. G. I. Budker, Atomnaya Énergiya, No. 5, 9 (1956).
4. D. Finkelstein and P. A. Sturrock, Plasma Physics, McGraw-Hill Book Co. (1961).
5. D. Finkelstein, In symposium: "Storage of Relativistic Particles" [Russian translation], Moscow, Atomizdat (1963), p. 171.
6. A. A. Vedenov, E. P. Velikhov, and R. Z. Sagdeev, Usp. fiz. nauk, LXXIII, 701 (1961).
7. L. D. Landau, ZhÉTF, 16, 574 (1946).
8. J. E. Drummond, Plasma Physics, by Editor J. Drummond, McGraw-Hill Book Co. (1961).
9. A. A. Vedenov, E. P. Velikhov, and R. Z. Sagdeev, Nuclear Fusion, 1, 82 (1961).
10. V. E. Zakharov and V. I. Karpman, ZhÉTF, 43, 490 (1962).
11. A. A. Galeev, V. N. Oraevskii, and R. Z. Sagdeev, ZhÉTF, 44, 903 (1963).

All abbreviations of periodicals in the above bibliography are letter-by-letter transliterations of the abbreviations as given in the original Russian journal. *Some or all of this periodical literature may well be available in English translation.* A complete list of the cover-to-cover English translations appears at the back of this issue.

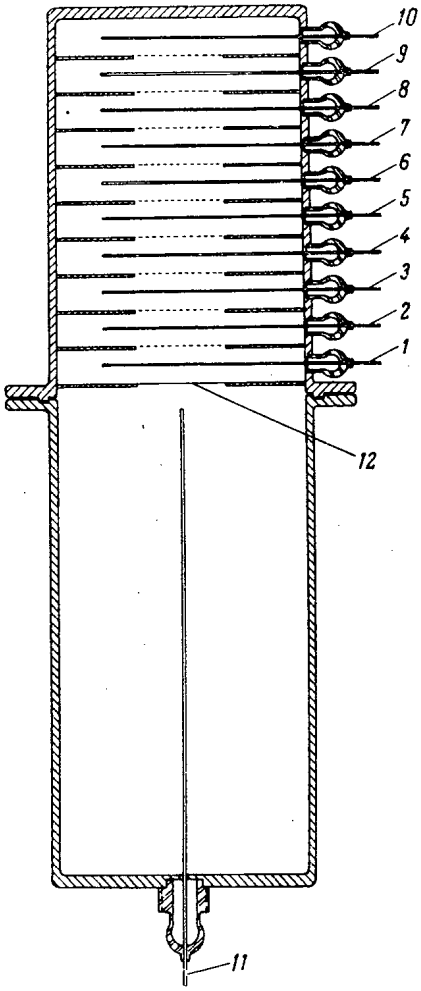

Fig. 1. Diagram of ionization chambers.

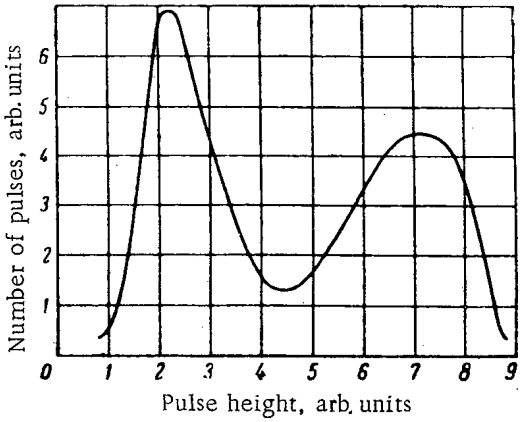

Fig. 2. Pulse height distribution in chamber 9.

$$v_i = \overline{(dn/dR)}_i \frac{\Delta Re}{C} = -\overline{(dE/dR)}_i \frac{\Delta Re}{WC}, \quad (1)$$

where ΔR is the length of a chamber; e is the charge on the electron; C is the electrical capacity of a chamber; W is the energy lost by a fission fragment in the creation of an ion pair.

A typical pulse height distribution in chamber 9, shown in Fig. 2, was obtained for fragments for thermal fission of U^{235} at 35 mm Hg total pressure of the filling gas, Ar + CH_4 (5%), in the chambers.

The following measurements were carried out with the help of a DMA-1024 two-dimensional pulse height analyzer having 32 channels along each axis [11]. Chamber 9 was kept connected to the input of one analyzer axis; the remaining chambers of the telescope were connected in turn to the input of the other axis. Thus, chamber 9 enabled one to distribute the fragments over 32 channels in accordance with their ionizing power, and the two-dimensional analyzer made it possible to follow the specific ionization from chamber to chamber for each group of fragments whose pulses from chamber 9 fell into the appropriate analyzer channel.

In Fig. 3 is shown typical pulse height distributions in the first eight chambers of the telescope from a group of heavy fragments whose pulses from chamber 9 fell in the sixth channel of the analyzer.

In analyzing the results, the pulse heights corresponding to the positions of the maxima of the distributions were considered values characteristic of the average specific ionization of the group of fragments. From these values, v(R) curves were constructed for all groups. The relationship $-dE/dR(R)$ for the fragments was computed from the experimental data for the distribution of v(R) in accordance with relation (1). To do this, the constant relating the quantities v(R) and $-dE/dR$ (R) was determined on the basis of data for the initial energies of the most probable light and heavy fragments (100.2 and 66.7 MeV, respectively [12]). The conversion coefficient was determined independently from both energy values, and the values agreed within 2%. For all other fragments different from the most probable, the average value of the coefficient was used in the calculations. The initial energy of the fragments was determined from the area under the $-dE/dR$ (R) curve. Measurements on the two-dimensional analyzer with chamber 11 enabled one to find the energy of fragments travelling in a direction opposite to that of chambers 1-10. To find the dn/dR (R) dependence, it was assumed that the average energy expended in the creation of an ion pair was the same for all fragments and amounted to 26.6 eV [3].

The dependence shown in Fig. 2 characterizes the distribution of fragments in ionizing power for normal gas pressure along a small portion of the track ΔR = 1.4 mm (range from the beginning of the track, 11-12.4 mm). Although this distribution resembles the two-group mass distribution of the fragments, it is not the mass distribution itself. The beginning of the distribution corresponds to the heaviest fragments, the first maximum to the most probable heavy fragment, and the second maximum to the most probable light fission fragment.

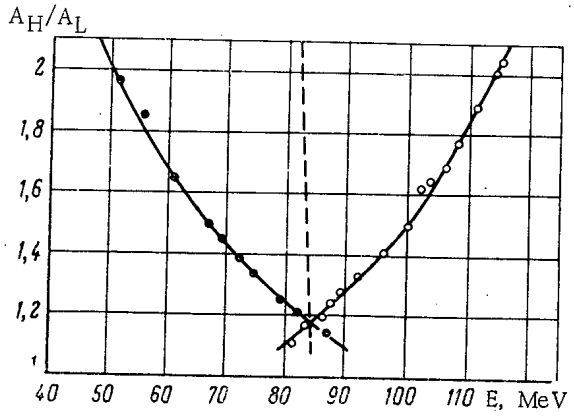

Fig. 5. Dependence of the most probable mass ratio for U^{235} fission fragments on the energy of one of the fragments (● – heavy, ○ – light fragment).

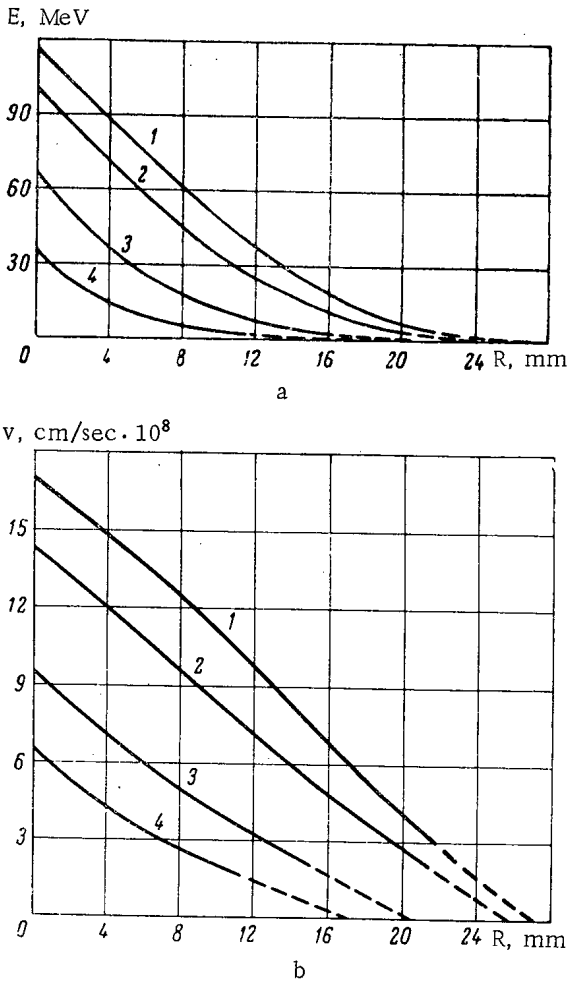

Fig. 6. Curves of energy (a) and velocity (b) along the track of fragments with different initial energies, MeV: 1) 115.5; 2) 100; 3) 67; 4) 34.

averaging over the experimental points. In Fig. 4, values are given for the most probable masses of the light, A_L, and heavy, A_H, fragments corresponding to the values found for the energies E_L and E_H. The mass was determined from the ratio of the initial energies of the fragments E_L/E_H. It should be pointed out at once that the mass was determined with poorer precision than the initial energy of the fission fragments because the error in this case is made up of the errors in successive measurements of the energies of both fragments emitted from the U^{235} layer in opposite directions. The largest error, approximately ± 10%, attaches to masses far from the most probable because of the low statistically effective count rate and partly because of the resolution of the chambers.

It is difficult to measure specific ionization out to the end of a track. The small maximum in the $-dE/dR$ (R) curve at the end of a fragment track, shown in Lassen's papers, was not investigated here. Because of this, the numerical results of the experiment have an additional error associated with the arbitrary extrapolation of the $-dE/dR$ (R) curve to the end of the fragment track.

Two experimental curves are shown in Fig. 5 which characterize the most probable fragment mass ratio for the emission of one of them with a given energy. Although the curves were obtained independently of one another, their inherent connection is completely clear. The curves have an almost symmetric shape. The line drawn in the center between the curves evidently characterizes the most probable energy falling to the share of one fragment, on the average, for fission with a mass ratio A_H/A_L.

Because fragments (for example, heavy ones) with the same initial energy can be obtained from fission with different mass ratios A_H/A_L, all the results obtained in the experiments should be referred to fragments with the most probable mass for a given energy.

It is clear from Fig. 4 that the light fragments differ from the heavy ones in the nature of the ionization along a track. Portions of the light fragment tracks with notably different rates of decrease in the quantity $-dE/dR$ characterize different rates in the loss of charge Z_{eff}. The ionization energy loss per unit length for the majority of the heavy fragments is greater than for the light fragments at the beginning of the tracks. This comparison could best be made if the specific ionization were represented as a function of velocity. For example, a comparison of specific ionization at identical fragment velocities directly characterizes their charges. Such a relationship was derived on the basis of the experimental data. To do this, curves were determined, first for the energy E, and then for the velocity V, along the track of fragments having different initial energies and velocities through the data for $-dE/dR$ (R). The data about the fragments are of interest in themselves. Curves of the functions E(R) and v(R) are given in Fig. 6 for four fragments. The upper and lower curves refer to the lightest and heaviest fragments, respectively, for which experimental data were obtained. The middle curves typify the most probable fragments on the light and heavy groups. Similar curves were obtained for fragments with other initial energies and velocities, and then the dependence of

3. F. Nasyrov, Atomnaya Énergiya, 16, 449 (1964).
4. N. Perfilov, Dokl. AN SSSR, 28, 5 (1940).
5. N. Lassen, Phys. Rev., 68, 142 (1945); Phys. Rev., 69, 137 (1946).
6. N. Lassen, Kgl. danske. Vid. selskab. Mat.-fys. medd., 30, 13 (1955).
7. C. Fulmer and B. Cohen, Phys. Rev., 109, 94 (1958).
8. N. Bohr, Phys. Rev., 58, 654 (1940).
9. N. Bohr, Phys. Rev., 59, 270 (1941).
10. N. Bohr, Penetration of Atomic Particles through Matter [Russian translation], Moscow, Izd-vo Inostr. Lit. (1950).
11. A. A. Rostovtsev et al., Atomnaya Énergiya, 11, 58 (1961).
12. Handbook of Nuclear Physics, Translated from the English, L. A. Artsimovich, ed., Moscow, Fizmatgiz (1963), p. 321.

All abbreviations of periodicals in the above bibliography are letter-by-letter transliterations of the abbreviations as given in the original Russian journal. *Some or all of this periodical literature may well be available in English translation.* A complete list of the cover-to-cover English translations appears at the back of this issue.

TABLE 2. Levels in Re Isotopes

Isotope	Resonance energy	$2g\Gamma_n$	
		this work	[7]
Re^{185}	2,156±0,019	4,3±0,2	6,6±0,1
	5,93±0,02	0,24±0,04	—
	7,18±0,03	1,6±0,3	—
	11,97±0,06	0,94±0,12	0,63±0,07
	12,9±0,07	0,9±0,1	0,72±0,08
	14,74±0,09	0,94±0,15	0,65±0,07
	21,46 _ 0,15 *	10,3±1,6	5,3±0,3
Re^{187}	4,41±0,01	0,41±0,09	0,64±0,10
	11,2±0,06	3,0±0,3	1,8±0,1
	16,2±0,10	0,73±0,10	0,44±0,04
	17,7±0,1	2,3±0,3	1,32±0,14
	18,5±0,1	0,7±0,1	0,52±0,05

* Unresolved level.

were also observedin rhenium with energies of 22.09 ± 0.07, 24.94 ± 0.07, 26.79 ± 0.08, 27.45 ± 0.09, 29.6 ± 0.1, 34.08 ± 0.10, 36.7 ± 0.2, 39.7 ± 0.2, 41.7 ± 0.3, 45.8 ± 0.3, 47.8 ± 0.3, 50.5 ± 0.3, 51.6 ± 0.3, 54.0 ± 0.3, 55.3 ± 0.4, 58.0 ± 0.4, 61.5 ± 0.4, 63.7 ± 0.4, 70.8 ± 0.4, 74.6 ± 0.4, 79.0 ± 0.5, 87.0 ± 0.5, 96.7 ± 0.5, and 108.0 ± 0.5 eV. It should be pointed out that the level at 27.45 eV belongs in Re^{185}, and the one at 39.66 eV in Re^{187}.

As far as the identification of higher levels is concerned, this is difficult to do at the resolutions with which we were working.

Data on the total neutron cross sections of rhenium in the resonance region have been published [4-7], parameters obtained in [5] being used for some of the resonances in [7]. It should be noted that the value of $g\Gamma_n$ for the

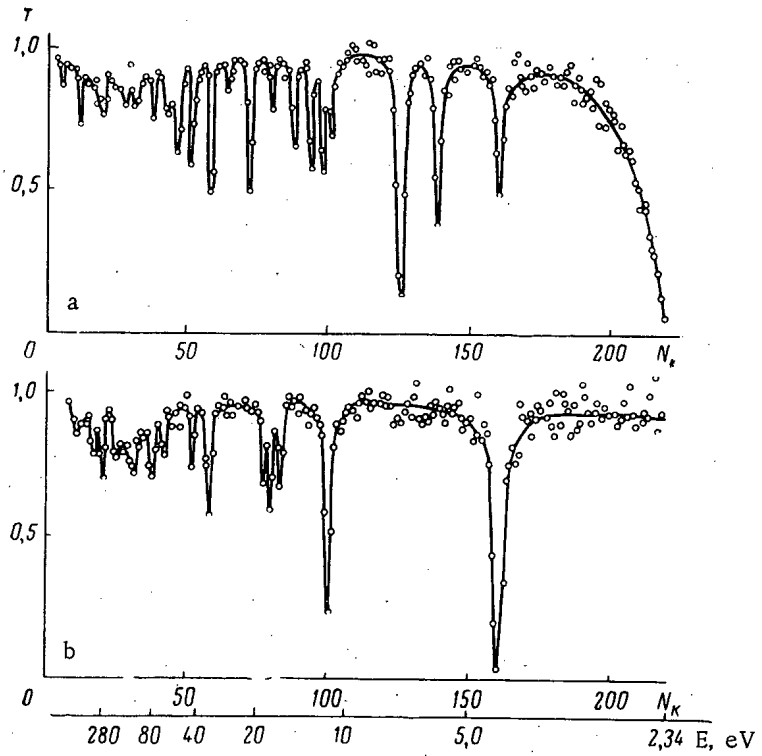

Fig. 1. Transmission of Re^{185} (a) and Re^{187} (b) samples.

average widths of the positive levels. The total cross section of Re^{185} at 2200 m/sec is 118 ± 2 b, and cross section of Re^{187} is 90 ± 2 b.

LITERATURE CITED

1. M. F. Vlasov and A. L. Kirilyuk, Ukr. fiz. zh., 8, 947 (1963).
2. V. V. Vladimirskii and V. V. Sokolovskii, In Proceedings of the Second International Conference on Peaceful Use of Atomic Energy [in Russian], Dokl. sovetskikh uchenykh, Vol. 1, Moscow, Atomizdat (1959), p. 519.
3. V. P. Vertebnyi et al., Atomnaya Énergiya, 12 (1962), p. 324.
4. Neutron Cross Sections, BNL-325, USA, AEC (1957).
5. G. Igo, Phys. Rev., 100, 1338 (1953).
6. V. P. Vertebnyi et al., Proceedings of the Working Conference on Slow Neutron Physics [in Russian], JINR, Dubna (1962), p. 8.
7. Suppl. to Neutron Cross Sections, BNL-325, USA, AEC (1961).
8. G. V. Muradyan and Yu. V. Adamchuk, Proceedings of the Working Conference on the Interaction of Neutrons with Nuclei [in Russian], JINR, Dubna (1964), p. 22.

$$\left.\begin{aligned} T_0 E\frac{d^2\Phi_0}{dE^2}+E\frac{d\Phi_0}{dE}+\Phi_0=c_0(\Phi_0-\Phi_1);\\ T_1 E\frac{d^2\Phi_1}{dE^2}+E\frac{d\Phi_1}{dE}+\Phi_1=c_1(\Phi_1-\Phi_0). \end{aligned}\right\} \tag{1.2}$$

Here

$$c_i=\frac{P_{i,\,1-i}}{\xi_i\,(1-P_{01}-P_{10})}\quad (i=0;\ 1), \tag{1.3}$$

where ξ_i is the characteristic constant of a heavy-atom moderator; T_i is the temperature of moderator i measured in the same units as the neutron energy. Because the scattering cross section $\Sigma_s^{(i)}$ for both moderators is independent of neutron energy, the magnitude of P_{ij} for plane and cylindrical geometries can be calculated, for example, with the help of expressions given in [10, 11]. In order to obtain a good approximation of Eq. (1.1) to the transport equation, we shall assume that $L_i\Sigma_s^{(i)}\leq 1$.

In this paper, Eq. (1.2), which was solved in [1] by calculating the energy moments of the neutron flux density, is solved by means of a Laplace transform, which is defined for the neutron flux density Φ_i as

$$\overline{\Phi}_i(t)=L[\Phi_i(E)]=\int_0^\infty dE e^{-Et}\Phi_i(E). \tag{1.4}$$

Considering the boundary conditions $\Phi_i(0)=0$, $\lim_{E\to\infty}\Phi_i(E)=0$ $(i=0,1)$, we can obtain equations for $\Phi_0(t)$ and $\Phi_1(t)$ from Eq. (1.2) which must be solved with the initial condition (for normalization of total flux)

$$\overline{\Phi}_0(0)=\overline{\Phi}_1(1)=1. \tag{1.5}$$

2. Solution of the Equation System

If we introduce

$$\psi_i=(1+tT_1)^2\overline{\Phi}_i\ \ (i=0;\ 1);\ u=\frac{t(T_1-T_0)}{1+tT_1}, \tag{2.1}$$

we obtain for ψ_0 and ψ_1 a system of differential equations which can be represented in the form

$$\left.\begin{aligned} u(1-u)\frac{d^2\psi_0}{du^2}+[1+c_0+c_1-(4+c_1)u]\times\\ \times\frac{d\psi_0}{du}-2(1+c)\psi_0=0;\\ u(1-u)\frac{d^2\psi_1}{du^2}+[1+c_0+c_1-(3+c_1)u]\\ \times\frac{d\psi_1}{du}-2c_1\psi_1=0. \end{aligned}\right\} \tag{2.2}$$

Solutions of the system of hypergeometric differential equations which satisfy the initial condition, Eq. (1.5) can be written in the form

$$\left.\begin{aligned} \overline{\Phi}_i(t)=\frac{1}{(1+tT_i)^2}\\ \times F\left(2,\ c_i;\ 1+c_0+c_1;\ \frac{t(T_i-T_{1-i})}{1+tT_i}\right);\\ \overline{\Phi}_i(t)=\frac{1}{(1+tT_{1-i})^2}F\\ \times\left(2,1+c_{1-i};\ 1+c_0+c_1;\ \frac{t(T_{1-i}-T_i)}{1+tT_i}\right), \end{aligned}\right\} \tag{2.3}$$

if one uses

the properties of the region, the spatial and energy dependence of the neutron flux density in the i-th region can be defined approximately by

$$\Phi(\mathbf{r}, E) \approx \sum_{i=1}^{N} \Phi_i(\mathbf{r})\, \chi_i(E). \tag{3.1}$$

It is understood that the spectra $\chi_i(E)$ are normalized to unity for the appropriate type of energy cutoff selected. Each spectrum $\chi_i(E)$ represents one group of neutrons whose contribution to neutron flux density or total neutron flux is determined by the functions $\Phi_i(\mathbf{r})$.

This method can be applied to the quasi-transport model discussed in the previous sections. In this model, the neutron absorption cross section is zero for each of the two components of the media considered so that neutron temperatures T_0 and T_1 correspond to the equilibrium spectrum $\chi_i(E)$ and to the Maxwellian spectrum:

$$\chi_i(E) = \frac{E}{T_i^2} e^{-\frac{E}{T_i}} \quad (i = 0;\ 1).$$

On the basis of Selengut's method, we obtain an expression for the neutron flux density

$$\Phi_i(E) = a_{i0}\chi_0(E) + a_{i1}\chi_1(E).$$

If the total neutron flux is normalized to unity, a solution is found in the form

$$\Phi_i(E) = \frac{1}{1+c_0+c_1}\{(1+c_{1-i})\chi_i(E) + c_i\chi_{1-i}(E)\}, \tag{3.2}$$

where i = 0, 1.

It is more practical to make a comparison of Selengut's approximate solution with the exact solution on the basis of integral characteristics where detailed calculations of the exact spectrum are not required. First, we form the neutron density moments

$$M_n^{(i)} = \frac{1}{n!}\int_0^\infty dE\, E^n \Phi_i(E).$$

Using the approximate solution Eq. (3.2), we obtain for m = 0, 1, 2, ...

$$M_n^{(i)} \approx \frac{n+1}{1+c_0+c_1}\{(1+c_{1-i})T_i^n + c_i T_{1-i}^n\}. \tag{3.3}$$

Correspondingly, we have for the exact solution

$$M_n^{(i)} = (n+1)\frac{\Gamma(1+c_0+c_1)}{\Gamma(n+1+c_0+c_1)}\sum_{\nu=0}^{n} \times T_i^\nu T_{1-i}^{n-\nu}\binom{n}{\nu}\frac{\Gamma(n-\nu+c_i)\,\Gamma(\nu+1+c_{1-i})}{\Gamma(c_i)\,\Gamma(1+c_{1-i})}. \tag{3.4}$$

Hence it follows that one can calculate the moments of the neutron flux density accurately by the approximate method only for n equals 0 and 1, and higher moments obtained by the use of Eq. (3.3) are incorrect. Using Eq. (3.2), one can obtain from Eq. (2.7) an expression for nuetron density or effective neutron temperature corresponding to the interrelation between density and neutron flux:

$$\frac{1}{\sqrt{T_i^{\text{eff}}}} = \frac{1}{1+c_0+c_1}\left(\frac{1+c_{1-i}}{\sqrt{T_i}} + \frac{c_i}{\sqrt{T_{1-i}}}\right). \tag{3.5}$$

It is necessary to compare this result with Eqs. (2.8) and (2.9).

A comparison of the results obtained by Selengut's approximate method with the exact solution shows that the approximate method leads to the correct result in many cases, especially when a strong interaction between neutrons and one of the two components of the medium under investigation predominates and when the temperatures of the two media are insignificantly different.

	Equations (2.8) and (2.9)	Equation (3.5)
T_0^{eff}/T_0	0.81	0.735
T_1^{eff}/T_1	0.69	0.643
T_0^{eff}/T_1^{eff}	1.17	1.14

On the other hand, the results that have been obtained point to the need for a critical approach to the interpretation of the results from relative integral measurements. Situations are possible where the theoretical and experimental results are in good agreement although the theoretical model reflects an actual situation rather poorly. A definite conclusion can only be reached on the basis of results from a large number of different integral experiments.

LITERATURE CITED

1. K. Meyer, Kernenergie, 4, 935 (1961).
2. D. Kottwitz, Nucl. Sci. and Eng., 7, 345 (1960).
3. M. V. Kazarnovskii, A. V. Stepanov, and F. L. Shapiro, In: Proceedings of the Second International Conference on the Peaceful Use of Atomic Energy [in Russian], Dokl. sovetskikh uchenykh, Vol. 2, Moscow, Atomizdat (1959), p. 651.
4. D. Selengut, Nucl. Sci. and Eng., 9, 94 (1961).
5. H. Hurwitz, M. Nelin, and G. Habetler, Nucl. Sci. and Eng., 1, 280 (1956).
6. H. Märkl, Nukleonik, Heidelberg, 4, 39 (1962).
7. A. Mockel and I. Devooght, Nucleonik, 4, 236 (1962).
8. A. Müller, Nukleonik, 2, 54 (1960).
9. W. Rothenstein, Nucl. Sci. and Eng., 7, 162 (1960).
10. J. Chernick, Genfer Berichte, 5, 215 P-603 (1959).
11. H. Kiesewetter, Kernenergie, 6, 106 (1963).
12. W. Magnus and F. Oberhettinger, Formeln und Sätze für die speziallen Funktionen der mathematischen Physik. Springer Verlag. Berlin, Cöttingen, Heidelberg (1948).

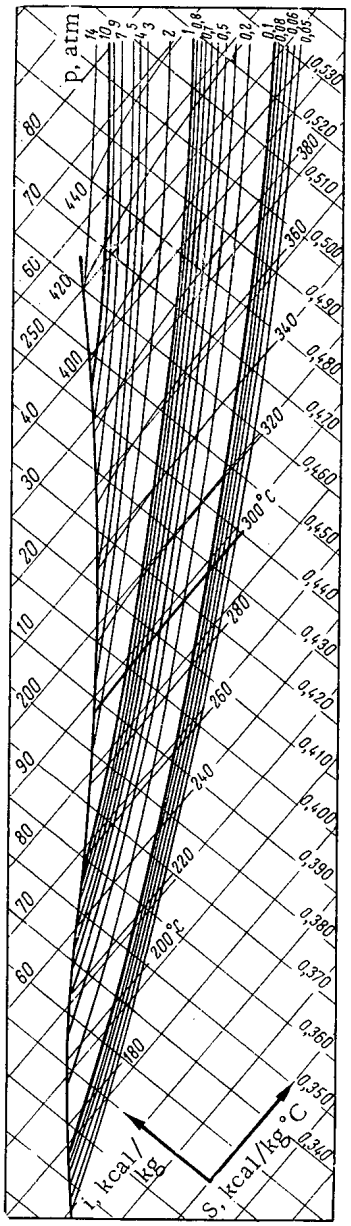

Fig. 1. i-s Diagram for diphenyl.

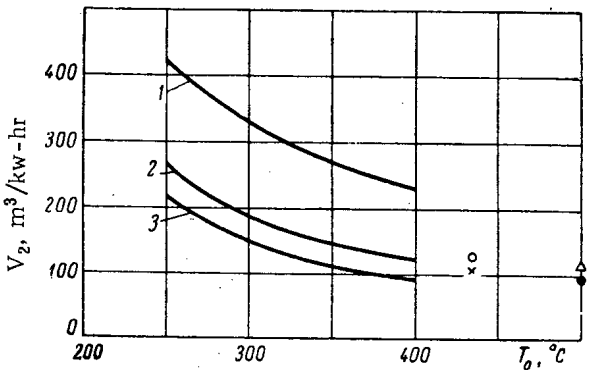

Fig. 2. Specific volume flow rate of vapor at turbine exhaust, plotted versus initial temperature of diphenyl. 1) Vacuum of 0.035 atm; 2) 0.07 atm; 3) 0.1 atm. ○) Turbine K-4-35; ×) turbine K-6-35; △) turbine K-25-90; ●) turbine K-50-90.

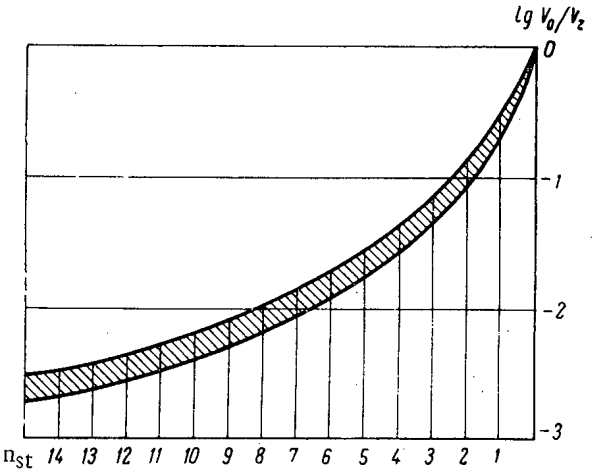

Fig. 3. Change of volume flow rate of vapor, plotted versus number of stages for condensing steam turbines.

volume flow rate of vapor in a diphenyl turbine, it is relatively easy to achieve sufficient length of the first-stage vanes.

Especial interest attaches to the subsequent stages, whose dimensions determine the limiting power. For condensing steam turbines, the maximum power is determined by the flow characteristics, though there is here also a certain difficulty in getting a smooth enough flow section.

To calculate the limiting power of a one-flow condensing turbine we use a formula from [9]:

$$N_{\max} = \frac{175}{\left(\frac{n}{1000}\right)^2} H_0 \eta_{0i} \eta_M \frac{c_z}{v_z} \text{ kw}, \quad (1)$$

where H_0 is the available heat transfer in the turbine in kcal/kg, n is the speed of the rotor in rev/min, c_z is the exhaust velocity of the vapor in m/sec, v_z is the specific volume of the vapor at the exhaust in m^3/kg, and η_M is the mechanical efficiency of the turbine.

6. For all the stages $\bar{x}_a = 0.5$.

From these assumptions we get

$$h_{ok} = 4\beta d_1^2 \left[1 + \left(\frac{l}{a}\right)^m\right]^2. \tag{4}$$

The mean available heat transfer per stage is

$$h_{o.av} = \frac{4\beta d_1^2}{a} \int_0^a \left[1 + \left(\frac{l}{a}\right)^m\right]^2 dl = 8\beta d_1^2 M(m), \tag{5}$$

where M(m) is the function plotted in Fig. 4. From the initial and final parameters of diphenyl vapor, we find V_0 and V_z, and from the graph in Fig. 3 we determine the number of stages required, n_{st}. Since

$$n_{st} = \frac{H_0}{h_{o.av}} = \frac{H_0}{2\beta d_z^2 M(m)},$$

therefore

$$d_z = \sqrt{\frac{H_0}{2\beta M(m) n_{st}}}. \tag{6}$$

The weight of vapor passing through the final stage, with axial exhaust, is

$$G_z = \pi d_z l_z c_z \frac{1}{v_z} = 0.523 \frac{H_0 c_z}{\beta M(m) n_{st} v_z}. \tag{7}$$

This equation shows that in this case the maximum flow rate through the final stage depends on the available heat transfer, in contrast to those turbines in which the limiting power is determined by the strength characteristics.

The limiting power of a diphenyl turbine is given by

$$N_{max} = G_z H_0 = 6.7 \left(\frac{1000}{n}\right)^2 \cdot \frac{H_0^2 c_z}{M(m) n_{st} v_z} \eta_{0i} \eta_M \text{ kw}. \tag{8}$$

Figure 5 gives the results of calculations from Eq. (8). It was assumed that $\eta_{0i} = 0.86$, $\eta_M = 0.96$, losses at exhaust velocity = $\xi_{E.V.} = 2\%$, and with n = 3000 rev/min in Eq. (8) the reducing gear efficiency $\eta_r = 0.98$. It is seen that, for the conditions assumed, the limiting power of a diphenyl heating turbine is very small.

In the range of parameters under consideration, we can take the isoentropy index K = 1.025. This corresponds to a critical pressure ratio $\varepsilon_* = 0.61$. From the values of K and ε_*, Fig. 6 plots the change in the parameters of the diphenyl vapor current versus $\varepsilon = (P_2/P_1)$.

Thus the diphenyl vapor reaches sonic escape velocity at a lower pressure ratio than that for steam. At the same temperature, the velocity of sound in diphenyl vapor is less than in superheated steam.

Our discussion of the properties of diphenyl as the working substance of a turbine shows that a turbine in a nuclear diphenyl heating set with power 20-50 MW must have the following characteristics:

1. Low rate of rotation (down to n = 1000 rev/min), so that a reducing gear must be used (lower speeds are inconvenient because of the increase in size of the turbine);

2. Two-flow construction in one casing, as owing to the low available heat transfer the number of stages is small;

3. Single-crown regulating stage (with nozzle vapor distribution);

4. Exhaust diffuser with strongly developed through-flow cross section.

The optimum vacuum and the coefficient of loss at exhaust velocity must be determined from a practical analysis of the plant is performance and its requirements. However, it may be said that, from the viewpoint of volume flow rate at the exhaust, the best vacuum of a diphenyl turbine should not exceed 0.07 atm.

A TEST-RIG STUDY OF THE STARTUP MODES OF THE I. V. KURCHATOV NUCLEAR POWER STATION, BELOYARSK

(UDC 621.039.514.23)

V. N. Smolin, V. K. Polyakov, V. I. Esikov, and Yu. N. Shuinov

Translated from Atomnaya Énergiya, Vol. 19, No. 3, pp. 261-268, September, 1965
Original article submitted September 18, 1964; in revised form, September 26, 1964

The results are given of an experimental investigation carried out on a test-rig of the hydrodynamic stability of the coolant flow in the channels of the first and second reactors of the Beloyarsk Nuclear Power Station. The choice of methods of startup of the Nuclear Power Station units, which are acceptable to the experimental final adjustments, is justified. The results are given of a study of the startup modes.

Channel type reactors are used in the I. V. Kurchatov Nuclear Power Station, Beloyarsk. Water boiling is accomplished in one group of channels and steam superheat in the other group of channels [1]. In the initial state of the reactor the superheat channels and the steam ducts are filled with water. During startup, it is necessary to free these channels from water and to convert to steam cooling of the superheat channels. As a result of this, preliminary heating and startup of the NPS units must be undertaken without an extraneous source of heat.

In the startup period, just as in the nominal mode of operation of the station, it is necessary to provide reliable cooling of the fuel elements (absence of a heat transfer crisis, assurance of hydrodynamic stability). Papers [2 and 3] were devoted to a study of the noncrisis cycles of cooling of the fuel elements by a steam-water mixture. The present paper describes the results of an investigation into the hydrodynamic flow rate stability of coolant in the channels in the boiling cycle; the problem is discussed of the transition of the superheat channels from the water cooling cycle to the steam cycle, with subsequent attainment of nominal parameters.

In order to carry out the investigation, experimental thermo-technological test-rigs were constructed, whose basic circuits corresponded to the technological circuits of the first and second units of the NPS [4]. The test-rig for the first unit consisted of two independent circuits, a closed loop and an open loop. Three evaporative channels are included in the first loop and one superheat channel is included in the second loop. The test-rig for the second unit is a closed single-loop circuit with an internal circulatory sub-loop. Two evaporative and two superheat channels were included in the loop. Chemically demineralized water was used as the coolant.

The experimental evaporative and superheat channels were made to natural size [1, 4]. In the evaporative channels, the coolant through the central tube was directed into the lower cap and then lifted upwards through six peripheral tubes, passed through the heating zone and entered the upper cap. The design of the superheat channels of the first unit of the NPS is similar to the evaporative channels. In the superheat channels of the second unit there is no central tube. The coolant moves downwards through three tubes and upwards through three tubes. The coil compensators for linear expansion in the evaporative and superheat channels of the first NPS reactor are located below the active zone and in the superheat channels of the second reactor they are above the active zone in the descending tubes.

The experimental channels, in contrast from the operating channels, have no fuel elements. The coolant in the experimental channels was heated by a low-voltage electric current over a length corresponding to the active zone of the reactor. All the tubes of the channels in the heated zone were connected in parallel with one another, by common current-feed contacts. The central tube of the evaporative channels was electrically insulated from the

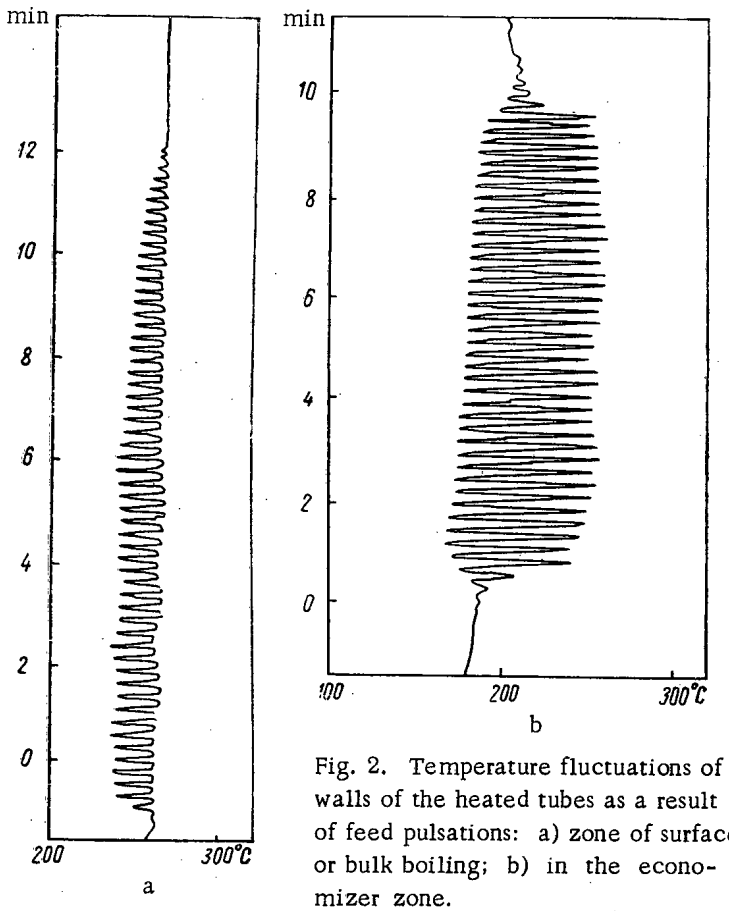

Fig. 2. Temperature fluctuations of walls of the heated tubes as a result of feed pulsations: a) zone of surface or bulk boiling; b) in the economizer zone.

lations per minute. Subsequent increase of the steam content again led to the creation of the pulsations. Secondary pulsations (see Fig. 1b) arising in the region of high steam contents were characterized by the considerable and quite high frequency (15-20 oscillations per minute).

Feed pulsations in the channel tubes were accompanied by temperature fluctuations of the tube walls over the entire length, with a frequency coinciding with the frequency of the feed fluctuations. In regions of low steam content, the temperature fluctuations of the walls in the upper sections of the heated zone (where surface or bulk boiling was observed) only occur on the side of reduction from the initial value (Fig. 2a); in the economizer zone it occurs on both sides of the initial value (Fig. 2b). The maximum amplitude of the temperature fluctuations of the walls were found to occur in the economizer zone of the channels, but did not exceed the temperature differences which the walls of the heated tubes have at a coolant temperature equal to the saturation temperature and to the channel inlet temperature. In the regions of high steam content, as a result of the generation of secondary pulsations, the temperature fluctuations of the walls in the upper sections of the heated zone were of a crisis nature and occurred only on the side of increase from the initial value. Thus, as a result of the investigation, two regions of pulsation modes are observed: a region of low steam content (x = 0-15%) and a region of high steam content (x = 25-80%).

Figure 3 shows curves, separating the zones of stable (upper curves) and pulsation (lower curves) operation of the evaporative channels of the second unit in the region of low steam content. It follows from the figure that with increase of pressure, the range of stable operation of the channels is extended, for a constant coolant feed rate. With increase of the feed rate the zone of nonpulsation operation is increased. An increase of power contracts the zone stable operation of the channels. The data given were obtained in channels with 6.2 mm diameter discs. In the channels of the first unit, with 4.2 mm diameter discs, no pulsations were observed over the entire range of feed rates investigated (700-2500 kg/h per channel) at pressures of 980 newton/cm^2 and above.

Secondary pulsations were observed with feed rates through a channel of less than 1000 kg/h, a pressure below 600 newton/cm^2 and a steam content at the channel outlet in excess of 25%. With increase of pressure, the pulsations originated at higher steam contents. For example, at a feed rate through the evaporative channels of the first reactor of 1000 kg/h and a pressure of 400 newton/cm^2, the pulsations originated at a steam content of 35%, and at a

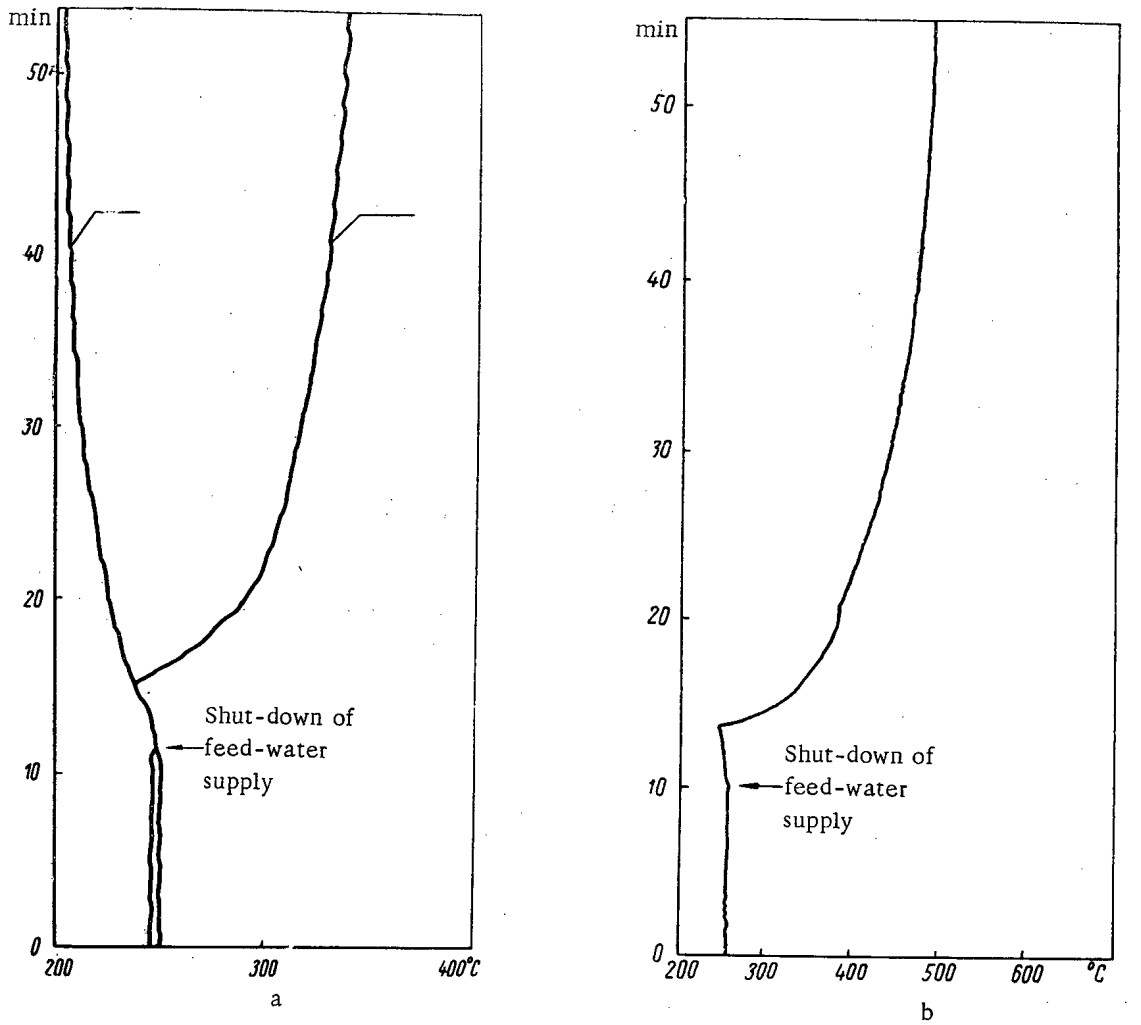

Fig. 4. Temperature changes in the transition cycle. a) Coolant temperature at inlet and outlet of superheat channels of the first reactor; b) wall temperature of heated tube.

that described in [5]. Essentially, it consisted in the following: the apparatus is heated up without boiling of the coolant in the first and second loops. After the water temperature attains a stationary value in the evaporators, the power is reduced and the supply of feed water in the loop is shut off. Water from the second loop is removed through the superheat channels. The pressure in the second loop falls, the water boils off, the steam-water mixture proceeds to flow out of the loop and, finally, a stable level is set up in the evaporators. The superheat channels are finally freed from water. Preliminary heating up of the second loop without boiling of the coolant enables it to be removed from the insert tubes of the superheat channels.

By studying the hydrodynamic instability of the feed rates in the evaporative channels, it was established that boiling in the primary circuit without inter-loop pulsations can be achieved only at pressures of 700-800 newton/cm^2. The dual-circuit technological test-rig system, just like the layout of the first unit of the NPS, enables any pressure whatsoever to be established independently in the primary circuit over the startup period as a result of the absence of boiling in the evaporative channels. This makes it possible to transfer the first circuit to the boiling cycle after purging the superheat channels and after the establishement in the second circuit of such a pressure at which, as a result of its transfer to the boiling cycle, the pressure in the first circuit should not fall below the stated limit.

The experiments were undertaken at an initial pressure in the first circuit of 1000 newton/cm^2 and in the second at a pressure of 300-400 newton/cm^2. After filling the loops with water, the specified pressure was created, the coolant feed through the channel was stopped and the heating was switched on. The test-rig was heated up to a water outlet temperature of 5-10°C below the saturation temperature. The power was then reduced to 3-4% of nominal and the supply of makeup water was shut off. The pressure in the loop dropped, which led to boiling of the water. At this instant, steam formation took place in the loop because of the heat of the first loop as well as the accumulated heat.

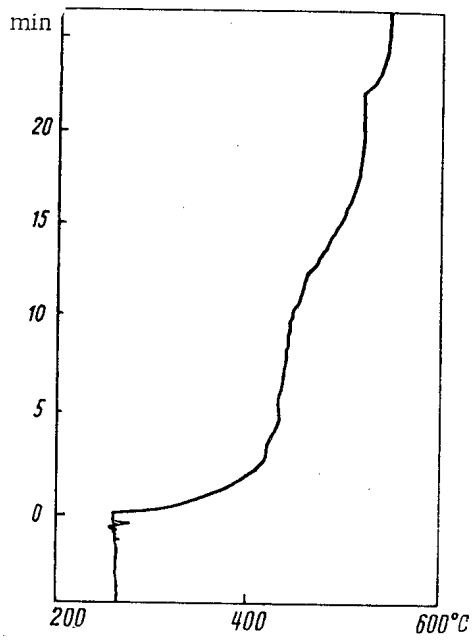

Fig. 7. Change of wall temperature of a heated tube of the superheat channel as a result of startup at reduced pressure.

In contrast from the circuit of the first unit of the NPS, the second unit has a single-loop circuit. The situation does not permit the startup method used for the first unit to be used to the full extent, since the large drop of pressure in the loop leads to the creation of feed pulsations in the tubes of the evaporative channels. Subsequent increase of power after purging the superheat channels from pulsating feeds in the evaporative channels, can lead to vortexing of the feeds and overburning of the fuel elements. Consequently, purging of the superheat channels must be carried out with the provision of a stable coolant supply in the evaporative channels.

For handling on the test-rig, the method was used of the gradual replacement of the water circulating through the superheat channels, first of all by a steam-water mixture and then by steam. This method was used in one loop of the First Nuclear Power Station [7]. The loop circuit contained evaporative and superheat channels. A certain supply of water was established through the evaporative channels and part of the water was directed into the superheat channels via the separator. The onset of superheating was accomplished by increasing the power prior to the instant of formation of the level in the separator without adjusting the coolant feed.

In our experiments, the required startup power was determined from the conditions for providing reliable purging of the superheat channels. This was dependent upon the necessity for ensuring the passage of a supply of steam through each ascending tube of any superheat channel up to the instant of purging the steam from them, which would generate a pressure drop between the lower cap and the composite collector, equal to or greater than the levelling pressure of the coolant column in the ascending tract of the channel [8].

Heating of the test-rig prior to obtaining water in the separator, located on the saturation line, and subsequent purging of the superheat channels was carried out at a pressure which ensures a nonpulsation cycle of operation of the evaporator channels. The initial supply of feed water was assumed to be such that the conditions were satisfied which would ensure stable supplies in the descending tubes of the superheat channels (see Fig. 3b). After heating up the test-rig prior to the production of water in the separator, located on the line of saturation, the feed water supply was reduced gradually. A steam-water mixture entered the superheat channels and finally, after the formation of the level in the separator, saturated steam entered. The level in the separator was formed by reducing the supply of feed water to an amount somewhat less than the amount of regenerated steam. After purging the superheat channels, they were observed by the temperature of the superheated steam, the temperature of the heated tube walls and the level in the separator. The investigation was carried out on one of the two parallel-connected superheat channels at pressures of 490 and 880 newton/cm^2. The main consideration was given to determining the conditions at which reliable cooling of the superheat channels is ensured in the startup period.

As a result of carrying out the experiment, it was established that with an adequate pressure differential a temporary stoppage of circulation occurred even in an isolated superheat channel. Figure 5a shows the plot of the change of pressure differential in a superheat channel as a result of the gradual replacement of water by steam, and Fig. 5b shows the plot of the change of wall temperature of the heated tubes in the same process. It follows from the diagrams that at a pressure differential equal to 4 newton/cm^2, the circulation through the channel ceased, but the wall temperature of the tubes increased. Periodically, according to the extent of the pressure reduction in the circuit beyond the channel, the circulation was resumed in a small interval of time. After formation of the level in the separator, the channel was free from water and the fluctuations of the pressure differential and of the wall temperature of the tubes ceased (Δp_{min} = 4 newton/cm^2).

Figure 6 shows plots of the change of pressure differential in the channel and of the change of temperature of the walls of the heated tubes during the gradual replacement, but at a high power level in comparison with the experiment for which the results are shown in Fig. 5. In this case, circulation of the coolant through the channel did not cease (Δp_{min} = 8 newton/cm^2). The small fluctuations of temperature of the tube walls are explained by the passage of steam locks and by their superheating.

VARIATION OF THE PROPERTIES OF BERYLLIUM DURING AGING

(UDC 546.45)

V. M. Azhazha, I. G. D'yakov, I. I. Papirov,
and G. F. Tikhinskii

Translated from Atomnaya Énergiya, Vol. 19, No. 3,
pp. 269-272, September, 1965
Original article submitted August 25, 1964; in revised form, December 28, 1964

The change in the residual resistance and mechanical properties of powder-metal beryllium as a result of its residual resistance and plastic characteristics of beryllium on the time and temperature of aging are generally similar. A significant increase in the plastic properties of beryllium can be achieved by heat treatment of hot-pressed beryllium under the optimum system and by the aging of other grades of beryllium.

The plasticity of beryllium in the region of "hot" brittleness at temperatures of 400-600°C may be substantially improved as a result of aging of the supersaturated solid solution formed when the metal is cooled after various technological treatments [1].

For a study of the kinetics of the process of solution of the superfluous phases during homogenization and deposition of these phases during aging, the use of the method of measuring the residual resistance of the samples is promising [2]. Thanks to its high sensitivity to structural changes, this method permits recording of the initial stages of the processes of evolution, both at the usual temperatures of aging (~700°C) and at reduced aging temperatures (~400°C). With the aid of a measurement of the residual resistance, it has been shown, in particular, that the effect of temperature of aging depends on the purity of the metal, increasing with increasing amount of impurities, and that even metal of maximum purity (99.96% Be) undergoes aging during suitable heat treatment. These circumstances should be taken into consideration in selecting the system of aging, which must be modified depending on the grade of metal.

The purpose of this work was to establish the effectiveness of the influence of aging on the mechanical properties of beryllium at increased temperatures, as well as the interrelationship between the mechanical characteristics of aged beryllium and its residual electric resistance.

As the starting material, we selected hot-pressed beryllium, technical purity, with the following content of impurities (according to the data of spectral and chemical analyses):

Fe	Al	Mn	Si	Cu	Ni	Cr	Mg	Ca	C	O	N
0,04	0,035	0,03	0,005	0,01	<0,002	0,004	<0,002	0,015	0,14	0,07	0,01

The density of the metal was equal to 1.844 g/cm^3. The average grain size in the initial samples was about 60 μ. Pressed metal with a relatively high content of impurities and a coarse grain, was selected as the object of investigation in order to determine the magnitude of the effect of aging under the most unfavorable conditions from the structural standpoint. As is well known, the aging only of fine-grained extruded beryllium had been studied previously.

The mechanical properties of the samples were determined in tensile tests on a vacuum machine designed by the Physicotechnical Institute, Academy of Sciences Ukrainian SSR, at a rate of loading of 5 kg/mm^2 [3]. Flat samples were cut out of blanks on an electroerosion machine, ground and polished. The electrical and mechanical characteristics were determined on the same samples. The relative residual resistance of the samples was measured according to the procedure described earlier [2].

Fig. 4. Photomicrograph of the site of cleavage of a homogenized sample; testing at a temperature of 600°C (×70).

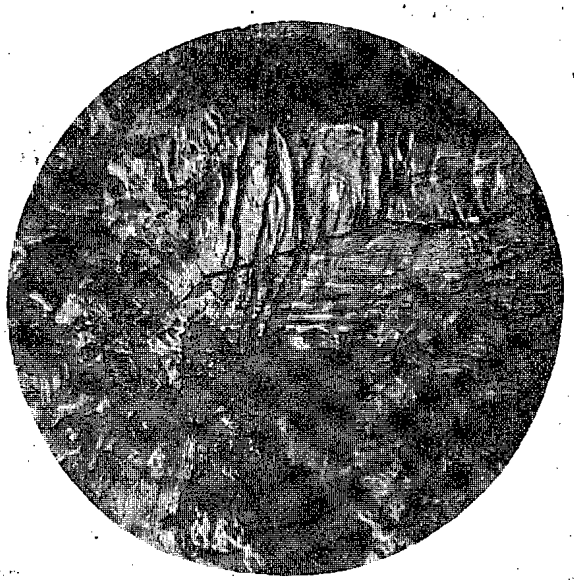

Fig. 5. Traces of slip and faults in aged beryllium; aging at 700°C for 100 h; testing at a temperature of 600°C (×200).

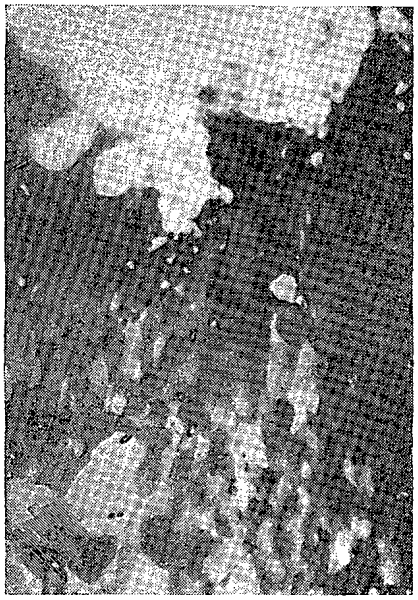

Fig. 6. Photomicrograph of the site of cleavage of aged sample; aging at 700°C for 40 h; testing at a temperature of 600°C (× 70).

The dependence of the relative constriction on the temperature was constructed according to average values, obtained in several experiments, which is due to the considerable dispersion of the experimental data. In view of this, let us mention that only the residual resistance of the samples, which is the most reliable characteristic of the state of the material, is characterized by high reproducibility of the results during aging. The relative elongation and especially the relative constriction vary from sample to sample within considerable limits, which is evidently due to the presence of surface or internal defects of macroscopic character, which have little influence upon the electric resistance. In other words, the residual resistance is a characteristic of the material, while the residual elongation and constriction are characteristic of the samples.

As can be seen from Fig. 2, the nature of the variation of all three quantities considered (δ, $\Delta l/l$, and ψ) as a function of the temperature of aging is similar in general outline. Heat treatment of beryllium at a temperature above the optimum (700°C) leads to a decrease in its plastic characteristics and simultaneously to a decrease in the relative variation of the residual resistance. Below 700°C, the process of liberation is very slow, while at higher temperatures the refinement of the solid solution is reduced. For metal of technical purity, containing various impurities, we can introduce the concept of the effective solubility curve, which is taken to mean the conditional integral dependence of the solubility of the basic impurities on the temperature. Since each impurity in beryllium is characterized by its own solubility parameters, the effective curve essentially represents some blurred region (band) of solubility. The value of the residual resistance is influenced precisely by this effective process of solution. An analysis of the residual resistance of samples aged under various conditions shows that in the investigated beryllium, the region of effective solubility lies above 850°C. Since the solubility of impurities in beryllium increases with increasing temperature, in accord with the lever rule, the equilibrium concentration of impurities in a solid solution will decrease with decreasing temperature of aging, while the number of deposited phases will thereby increase. This circumstance sets an upper limit to the optimum temperature of aging. Its lower limit, as was indicated, is the diffusion mobility. Hence, although aging below the optimum temperature (700°C for the investigated beryllium) theoretically might lead to a further in-

GAMMA AND NEUTRON DOSIMETRY IN NUCLEAR REACTORS BY MEANS OF COLORED POLYVINYL ALCOHOL FILMS

(UDC 539.1.083)

Ya. I. Lavrentovich, A. I. Levon, G. N. Mel'nikova, and A. M. Kabakchi

Translated from Atomnaya Énergiya, Vol. 19, No. 3, pp. 273-276, September, 1965
Original article submitted October 27, 1964

It is shown that polyvinyl alcohol films containing methylene blue which become discolored under the effects of radiation are suitable for gamma and neutron radiation dosimetry in nuclear reactors. The degree of discoloration varies linearly with the dose in the 10^4-10^6 rad range and, over a broad range of values, is practically independent of variations in linear energy transfer, dose rate, and temperature. Films containing boric acid in addition to the dye can be used for recording thermal-neutron doses in the 10^{12}-10^{14} neutrons/cm^2 range. The measurement error is within ±10% in every case.

The most accurate data on the magnitude of absorbed doses of ionizing radiation can be obtained by calorimetric methods, which are fairly complicated and not sufficiently versatile. In nuclear reactors the gamma-ray and neutron doses may also be determined by a number of chemical methods [1-3], based on the use of systems in which the degree of chemical changes is independent of the type and energy of the impinging radiation and depends only on the amount of energy absorbed. However, the systems used in these methods are liquids, and working with them is rather difficult.

In the present study we investigated the possibility of determining the gamma-ray and neutron doses in nuclear reactors by using polyvinyl alcohol films colored with methylene blue. To prepare the film, a mixture of 200 cm^3 of a 10% aqueous solution of polyvinyl alcohol and 40 cm^3 of a 10^{-3} M aqueous solution of methylene blue were poured onto a horizontal glass plate measuring 60 · 31 cm , which was shielded from dust. The plate was carefully washed with soda water and then dried, and before pouring the mixture of solutions, we rubbed the plate with cotton-wool dipped in ethyl alcohol. We used VTU M-582–55 industrial polyvinyl alcohol purified by reprecipitating it three times from an aqueous solution by means of methyl alcohol. The polyvinyl alcohol contained practically no acetate groups and was characterized by a high degree of polymerization: P = 2000. The solutions of analytically pure methylene blue (without any additional purification) were prepared with ordinary distilled water. Most of the moisture was removed by evaporating for 5-7 days at room temperature, after which the film was easily removed from the glass surface and kept in a desiccator over calcined calcium chloride until it reached constant weight. By this method we obtained solid, uniformly colored films with a thickness of about 90 μ. Specimens measuring 4 · 1 cm were used for the irradiation.

The thickness of the films was determined with an MBI-8M microscope. The intensity of coloration was measured with an SF-4 spectrophotometer. The films were irradiated with Co^{60} gamma quanta on equipment installed at the Institute of Physical Chemistry of the Academy of Sciences of the Ukrainian SSR, with 14 MeV deuterons and 28 MeV helium ions on the cyclotron of the Institute of Physics of the Academy of Sciences of the Ukrainian SSR,* and with gamma rays and neutrons in the VVR-M nuclear reactor of the same Institute. When the films were irradiated in the nuclear reactor and in the Co^{60} equipment, they were placed between polyvinyl alcohol plates 4 mm

* The films were irradiated in the cyclotron by V. A. Pashin, to whom the authors express their sincere gratitude.

TABLE 2. Radiation Yield Values Required to Restore the Dye after Various Types of Irradiation

Type of radiation	Radiation energy, MeV	Linear energy transfer, keV/μ	Dose rate, rads/sec	Radiation yield, molecules/100 eV
Co^{60} α-radiation	1.25	0.2	10-1000	1.80 ± 0.05
Gamma and neutron radiation from nuclear reactor*	–	–	6000	1.70 ± 0.09
Deuterons	14.0	7.5	10,000	1.70 ± 0.08
Helium ions	28.0	30.0	10,000	1.60 ± 0.09

* According to A. Ya. Denisenko's data, the contribution of neutrons to the total dose determined by chemical methods [2, 6] was 28 ± 5%.

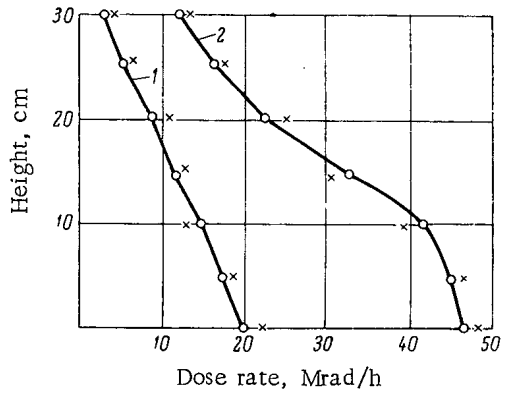

Fig. 3. Distribution of dose-rate values along the height of the channels of the VVR-M reactor: 1) measurements in channel 7/60 at a power of 1 MW; 2) measurements in channel 95/60 at a power of 2 MW; O) determined by calorimetric method; X) determined by means of films; the first experimental point was obtained 3 cm above the center of the active zone of the reactor.

Figure 2 shows how the optical density of the films at 660 mμ varies as a function of the Co^{60} gamma-ray dose at dose rates of $10\text{-}10^3$ rad/sec; the repeatability of the results is quite satisfactory (within ± 3%). It is clear that the degree of discoloration of the dye is a linear function of the dose in the $10^4\text{-}10^6$ rad range. The sensitivity and accuracy of measurements at doses of up to 10^5 rad are considerably improved when the film thickness is increased and the dye concentration is decreased. Thus, we can obtain films for measuring doses starting from 10^3 rad and, if we introduce various additives [5], even as low as 1 rad. For measuring doses higher than 1 Mrad, other dyes must be used instead of methylene blue. We will evidently be unable to obtain films suitable for measuring doses higher than 10 Mrad, owing to the specific nature of the chemical processes taking place in polyvinyl alcohol when it is irradiated.

When the film is irradiated with deuterons, helium ions, and gamma and neutron radiation from a nuclear reactor, the degree of discoloration of the dye varies linearly with the dose in the $10^4\text{-}10^6$ rad range, just as it does when the film is irradiated with Co^{60} gamma rays. The values of the radiation yields of the discoloration process when the dyed film is subjected to different types of radiation, as calculated from the angles of inclination of straight lines, are shown in Table 2, from which it follows that variations of the linear energy transfer between 0.2 and 30 keV/μ and of the dose rate between 10 and 10^4 rad/sec have little effect on the value of the radiation yield of the discoloration.

Specially designed experiments have shown that a temperature variation of −196°C to +50°C during irradiation has no effect on the value of the radiation yield.

The degree of discoloration of the dye is related to the magnitude of the dose (in rads) by the formula

$$D = 7.88 \cdot 10^3 \frac{S_0 - S}{l}, \quad (1)$$

where S_0 and S are the optical densities of the film before and after irradiation, respectively; l is the thickness of the film (cm).

It follows from the equation that in order to determine the dose by means of colored polyvinyl alcohol films, we need know only the degree of discoloration of the films resulting from the irradiation, since the thickness of the film can be standardized. As the absorption band is in the visible part of the spectrum, the degree of discoloration can be determined not only with a spectrophotometer but also with a photoelectrocolorimeter or colorimeters of different design, including the simplest kinds. If we know the dose range in which we expect to make the measurements, then the degree of discoloration, and consequently the magnitude of the dose, can be determined visually by comparing the color of the films with a color scale. Operators require no special training to make these measurements. It is well known that if the color scale is properly selected, the visual determinations will be accurate to within ± 5%.

TWO GENETIC TYPES OF POSTMAGMATIC THORIUM-RARE-EARTH DEPOSITS

(UDC 553.3/.4)

V. A. Nevskii and P. S. Kozlova

Translated from Atomnaya Énergiya, Vol. 19, No. 3,
pp. 277-281, September, 1965
Original article submitted August 13, 1964; in revised form, January 6, 1965

Two genetic types of postmagmatic thorium-rare-earth deposits have been distinguished. One is associated with surface ore channels, the other with plutonic bodies. The first type displays a close positional connection with the parental magmatic rocks, formed at shallow depths. These deposits have complex successional phases and polymineral compositions; the vertical extension of mineralization is very small. Deposits of the second type do not have close positional connections with the magmatic rocks which were formed at considerable depths and at considerable distances from the ore channels. The mineral compositions of the ores are relatively simple. The vertical extension of mineralization is several hundred meters, the mineralization type displaying persistence with depth.

In the present work we have made a detailed study of two types of postmagmatic thorium-rare-earth deposits. The first is regarded as a thorium-rare-earth deposit, the other as a thorium-beryllium-rare-earth-lead-zinc deposit—a more complex type than the former.

The characteristic feature of the structural-geologic position of thorium-niobium-rare earth deposits in their location in the marginal areas of selvages of the Pre-Cambrian crystalline basement among Paleozoic strata, in folded belts. The country rocks are ancient metamorphic series, including ancient gneissose granites, breached by nongneissose aplites, porphyrites and lamprophyres. The metamorphic rocks are generally crumpled into tightly pinched isoclinal (often flattened) folds and cut by numerous faults. The ore bodies consist of simple or complex quartz and quartz-carbonate veins with aegirite and glaucophane and subordinate ore minerals (Table 1).

These deposits were formed in a single stage, consisting of four phases: quartz, magnetite-carbonate-quartz, quartz-carbonate-sulfide and barren quartz-calcite. The bulk of the groundmass of the ore and vein minerals is related to the first and second phases; there is distinct evidence of the third phase but very little evidence of the fourth. In the first mineralization phase, practically the only mineral deposited was quartz, containing traces of zircon and wolframite (Fig. 1). The second phase is marked by an abundance of various vein and, in particular, ore minerals. The latter include the principal valuable components of the deposit: rare earths, niobium and thorium (monazite, ilmenorutile, ferrithorite, orthite, carbonates, and fluocarbonates of rare earths, etc.). The third phase is also marked by a great variety of ore and veing minerals, but the actual content of these is very small. The main fraction consists of vein minerals (quartz, calcite, fluorite, siderite, and a very small amount of barite). Late quartz and calcite were deposited in the fourth phase.

TABLE 1. Mineral Composition of Thorium-Niobium-Rare-Earth Deposits

Minerals	Main	Secondary	Rare
Vein	Quartz, calcite, siderite, aegirite, glaucophane	Biotite, microcline, fluorite, barite, muscovite, chlorite	Prehnite, tourmaline
Ore	Magnetite, hematite, carbonates and fluocarbonates of rare earths, ilmenorutile	Pyrite, ferrithorite, galena, molybdenite, rutile, thorite, titanomagnetite, orthite, apatite	Wolframite, sphalerite, chalcopyrite, gold, zircon

TABLE 2. Mineral Composition of Thorium-Beryllium-Rare-Earth-Lead-Zinc Deposits

Minerals	Main	Secondary	Rare
Vein	Quartz, biotite, albite, orthoclase, muscovite, sericite, fluorite, chlorite; carbonate rocks also contain vesuvian, garnet, diopside, aegirite-augite, calcite, ankerite, siderite, manganosiderite	Microcline, epidote	Topaz, tourmaline, actinolite, opal, chalcedony, barite
Ore	Pyrite, pyrrhotine, galena, sphalerite, molybdenite, monazite, parisite, bastnäsite, ferrithorite, cassiterite, xenotime, yttrofluorite, cyrtolite, malacon, magnetite, epidote	Chalcopyrite, arsenopyrite, bavenite, jamesonite, stannite, marcasite, cleiophane, wurtzite, epididymite and dudidymite, hematite, ilmenite, ferrihutonite, thorite, rutile, ambatoarinite, ancylite, calcioancylite, fluocerite, miserite, zircon, apatite	Boulangerite, pyrargyrite, stephanite, prousite, cosalite, polybasite, franckeite; native minerals – lead, bismuth, silver, tin, cinnabar, scheelite, wolframite, stannite, columbite, beryl, rutile, bismuthite, orthite

ferent compositions, while in others they are Lower Paleozoic carbonate or carbonate-argillaceous beds. They are usually pinched into tight, isoclinal (sometimes flattened) folds. Folded deformations, including dome-shaped folds, of less distinct character, are occasionally observed.

The ancient strata in these ore fields are breached by igneous rocks of different age. They include large granitoid massifs of the batholithic type with accompanying series of small intrusives and vein rocks and fissured intrusives (younger than the other tectonomagmatic cycle) of subalkaline granitoids and alkaline minor intrusions of diverse type.

These deposits have an abundance of faults, some being deep and often controlled by the fissured intrusives. The ore bodies are usually located at the margins of the alkaline and subalkaline rocks or in their exocontact zone. They contain vein and vein-shaped bodies located in some cases in individual complex shear joints or fractures, and in other cases in systems of these joints; they also contain irregular metasomatic bodies at the nodes where the fissures intersect or join; stockworks, lenses, pockets and tubular bodies with different cross sections are also found. The ore bodies in the exocontact of the massifs often display a distinct change in morphology with depth over short vertical ranges (for example, the lens-like bodies at the top pass into vein-shaped bodies at the bottom). Marked changes are also observed in the ratios between the simple fractures and shear joints over short vertical distances. The number of simple fractures decreases markedly (sometimes to nearly half) with depth, owing to the increase in the number of shear joints.

It will therefore be seen that in the pre-ore and ore-depositional period of formation the deformation conditions of the country rocks varied over fairly short vertical distances (200-400 m).

Ores of the thorium-beryllium-rare-earth-lead-zinc deposits have complex mineral compositions (Table 2). The main vein minerals of these deposits are quartz, biotite, albite, orthoclase, muscovite, sericite, fluorite, and chlorite. Skarn minerals – vesuvian, garnet, diopside, aegirite-augite – and also calcite, ankerite, siderite, manganosiderite occur extensively in deposits correlated with carbonate rocks. The main ore minerals include pyrite, pyrrhotine, galena, sphalerite, molybdenite, monazite, parisite, bastnäsite, ferrithorite, cassiterite, xenotime, yttrofluorite, cyrtolite, malacon, mangetite, and phenacite. In some deposits pyrrhotine is found extensively in place of pyrite, and epididymite and eudidymite are found in the beryllium minerals.

The deposits were formed in two stages, separated by a period of introduction of later differentiates of subalkaline and alkaline rocks. Each stage consisted of several phases. In deposits in carbonate rocks postmagmatic mineral formation began with formation of vesuvian-pyroxene-garnets and aegirite-augite skarns, while in other deposits it began with deposition of pegmatoid quartz containing cyrtolite, thorite and other minerals. This was followed by a quartz-muscovite-sericite phase. In most cases the mineralization of the first stage has virtually no significance, but in some deposits formation of thorium-beryllium-rare earth ores is associated with quartz-muscovite-sericite phase.

The second stage of ore deposition consists of four to five phases. In deposits where thorium-beryllium-rare-earth mineralization is associated with first-stage mineralization these phase reflect the formation sequence of sulfide ores. The following phases (from early to late) are distinguished: cassiterite-arsenopyrite, pyrrhotine, sphalerite-galena and barren carbonate. In other deposits albite, biotite-monazite, ferrithorite-orthoclase, and sulfide-quartz phases are distinguished (Fig. 2).

The thorim-beryllium-rare-earth-lead-zinc ores of practical interest are mainly associated with the second, third, and fourth phases of the second stage. Rare earths of the cerium group (which form 55-60% of the total rare earth content) were mainly deposited in the biotite-monazite phase, and those of the yttrium group (40-45%) in the later, ferrithorite-orthoclase phase. The sulfide mineralization was mainly formed in the sulfide-quartz phase.

During ore formation the subalkaline granitoids and alkaline rocks were subjected to gneissification, albitization, orthoclasization, serpentinization, chloritization, and quartzification; the crystalline schists underwent biotitization and chloritization. Skarning, fluoritization, quartzification, ankeritization, and sideritization occur extensively in the carbonate rocks.

Rhythmic zoning is observed in the distribution of the mineralization products with respect to the roof of the parent intrusives. In their indocontact zone or its immediate vicinity in the adjoining rocks we usually find products of the high-temperature mineralization of the first stage or of early phase of the second stage. The main thorium-rare-earth mineralization is located at some distance from the contact, while the sulfide and beryllium ores lie at still greater depths. Products of the barren mineralization of the final phase generally lie in the end flanks of the ore zones. Similar changes in mineralization are observed in the vertical section. Appreciable changes in the type of mineralization with depth are observed in vertical extensions of 100-150 m, sometimes in even shorter ranges. The over-all vertical extension of mineralization varies from 250-300 to 400-450 m, and that of the whole postmagmatic mineralization from 400 to 650 m. In the case of the fissured intrusives the maximum distance of the late mineralization from outcrops of the parental subalkaline and alkaline rocks reaches 2-2.5 km, while near the stocks it is ~1 km.

The individual ore bodies of these deposits were mainly formed by a combination of mineralization of contiguous phases. Combinations of first- and second-stage mineralization within an ore body are less frequent.

A reconstruction of the geologic section as it was during formation of the thorium-beryllium-rare earth-lead-zinc deposits, and indirect data on the deformation characteristic of the country rocks (extensive occurrence of pre-ore and ore-contemporary breccia in the fault zones), indicate that these deposits were formed at shallow depths (500-600 and 1000-1200 m).

The thorium-beryllium-rare-earth-lead-zinc deposits have close positional connections with the subalkaline and alkaline massifs and are affected by the zoning of the mineralization around the latter. Accessory minerals of the subalkaline and alkaline rocks, such as zircon, cyrtolite, apatite, fluorite, ferrithorite, monazite, cassiterite, molybdenite, pyrite, galena, etc., are important ore minerals of these deposits. The alkaline and subalkaline rocks, and the related deposits, are of similar age and usually controlled by the same faults. It may therefore be inferred that a genetic relationship exists between the thorium-beryllium-rare earth-lead-zinc deposits and subalkaline granite and alkali syenites.

It will be seen that the thorium-niobium-rare-earth deposits were formed at considerable distances from the parent ore chamber, which probably developed at considerable depths from the surface (several kilometers or tens of kilometers). On the other hand, thorium-beryllium-rare-earth-lead-zinc deposits are directly associated with the parent intrusives and are evidently related to ore channels formed at shallow depths and near the mineralizations.

$$2(T_p + P) = \text{minimum;} \quad (4)$$

$$T_s + A_T + M = \text{minimum;} \quad (5)^*$$

$$K_A + T_e + A_T = \text{minimum,} \quad (6)$$

where T_p, T_s, and T_e are the costs of transporting the agricultural product, the radiation source and the plant, respectively, in rubles; P is the cost of loading and unloading the agricultural products to be irradiated, in rubles; A_T is the cost of radioactivity losses during transport, in rubles; M is the cost of assembling and dismantling the radiation sources in the plant, in rubles; and K_A is the administration costs of the operatives, in rubles.

The radiation utilization factor k_{ut} is an important index on which depends the total activity of the sources and thus their capital and running costs [3]. The formula which gives it is valid only with continuous irradiation. For calculating the source efficiency k_{true} in industrial plant, it is therefore necessary to make a correction equal to the difference between the half-life T and the standstill time t during this period, divided by the half-life:

$$k_{true} = k_{ut}\frac{T-\tau}{T} = 0.16\frac{Dn}{AE_\gamma}\cdot\frac{T-\tau}{T}\ \%, \quad (7)$$

where D is the dose required in r; n the productivity of the plant in g/sec; A the total activity of the sources in curie; and E_γ the radiative energy emitted by the source per single decay, in MeV.

Using the basic formulae for determining the economic efficiency of a new technology, given in [1, 2], and allowing for the above features of the indices for plant with radioactive sources, we derived the relation between the main technical parameters and the economic indices of methods for the irradiation of various agricultural products. The equation found was

$$\text{SDPn} = 2.25\cdot 10^{-2} k_{ut} E_\gamma m [T_N(C_1 - \bar{C}_2) + K_1 - \bar{K}_2] \quad (8)$$

or, allowing for standstill time,

$$\text{SDPn}\ (T-\tau) = 2.25\cdot 10^{-2} k_{true} E_\gamma T m [T_N(C_1 - \bar{C}_2) + K_1 - \bar{K}_2], \quad (9)$$

where P is the yearly productivity of the plant; m the number of hours' work per year; T_N the branch norm period for the profitability of additional capital expenditure, in years; K_1, $\bar{K}_2$ the capital investment for the basic and new variants (in the latter case, without expenditure on the radiation source in use), in rubles; C_1, $\bar{C}_2$ the net yearly production costs with these variants (in the latter case without expenditure associated with the use of the radiation source), in rubles; and n a coefficient equal to

$$T_N\left(\frac{1}{T} + 1 - e^{-\frac{0.693\cdot 1}{T}}\right) + 1.$$

These equations can be used to investigate and determine the optimum values for choice of the most economically efficient type of plant. If the values found are affected by other constant factors, the mean values of the function are found by the method of correlation, by solving a system of normal equations obtained by the method of least squares. For solving these equations it is more convenient to use graphical methods.

Let us consider these methods. In many references [4] it is shown that certain doses of gamma rays on plant seeds before planting will later (during germination, growth, and ripening) cause alterations in chemical exchanges which improve the plants' properties (reducing the vegetation period, increasing yield and improving the quality of the food and raw-material content).

To test the method in industrial conditions, the Latvenergo Works, on an assignment from the Institute of Biophysics of the USSR Academy of Sciences, prepared "GUPOS," an experimental unit for pre-sowing irradiation of vegetables and grain (cost 57,000 rubles, total activity of Cs^{137} sources equal to 800 g-equiv Ra). Calculations confirmed the efficiency of this method in agriculture. The additional capital costs for the GUPOS installation paid for themselves in one season by reducing the net cost of production of the crops by 8-16% and increasing the output per

* A type of radiation equipment consisting of several stationary constructions (biological shielding and plant) and one radiation source which is moved from one construction to another.

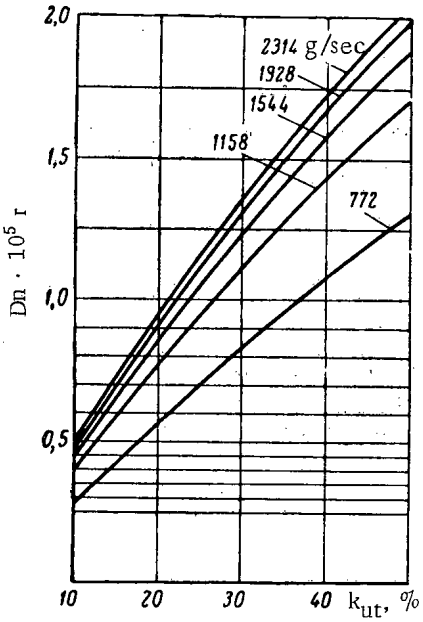

Fig. 3. Nomogram for determining the economically efficient types of plant for irradiation pasteurization of meat (T_N = 6 years) versus radiation dose D and radiation utilization factor k_{ut}, with plant working 7200 h per year and various productivities.

Using the suggested methods and graphical analysis of the principal technical-economic indices of radiation plant, we calculated and constructed nomograms for determining the optimum parameters of industrial plant for radiation disinfestation of grain and for improving the keeping capacity of perishable products. The norm for the period over which capital costs must pay for themselves was taken as five to six years [2].

From the nomograms (Figs. 1 and 2) it follows that a plant for irradiation disinfestation of grain will be economically efficient if, for plant productivity of 50-60 t per hour and costs of 75-90 kop. per g-equiv Ra of the Cs^{137} radiation source, the radiation utilization factor is 35-40% on average. For comparison we took the currently cheapest chemical method of disinfection of grain (methyl bromide). The first graph (Fig. 1) can be used to analyze the efficiency of this method for given plant productivity and various yearly working times; the second (Fig. 2) does the same for various productivities and given yearly working times. From these nomograms we can calculate the numerical values of the parameters which secure efficiency of the radiation method of grain treatment.

Owing to the varied natures of meat products (beef, pork, poultry, etc.), different radiation doses are required for their pasteurization. To determine the efficiency of the radiation method of treating meat products, it is therefore necessary to study how the basic technical-economic indices of the plant vary with the radiation dose of the objects. This is plotted in Fig. 3. The curves show that the method will be more efficient than freezing if the radiation dose does not exceed $1.5 \cdot 10^5$ r for mean productivity 5 t/hr, radiation utilization factor about 40% and cost of radiation source about 75-90 kop. per g-equiv radium from Cs^{137}.

The cost of irradiation sterilization of meat products is higher than that of autoclaving. However, if we consider the main advantage of the method – that it does not need heating – we see that by using nonheatproof packaging (plastic film) the radiation method can be made useful in food production. We must bear in mind the fact that irradiated products keep their nutritive value better than those treated by heating.

SUMMARY

1. The authors devise a method and draw graphs for determining the economic efficiency of gamma-ray isotope units for use in the production and treatment of agricultural products.

2. Taking concrete examples, they discuss the economic efficiency of nuclear techniques and give recommendations on the optimum values of the parameters of industrial gamma-ray isotope sources.

3. From their analysis they suggest that the question of reducing the distribution prices of radiation sources with high total activity should be considered as one of the conditions for improving the efficiency of radiation technique.

4. It is emphasized that it would be profitable to irradiate several different types of product with industrial plant based on Co^{60} and Cs^{137}, to avoid losses due to nonproductive decay of the radioisotopes.

5. It is suggested that, in the construction of industrial plant for seasonal treatment of agricultural products, use should be made of short-lived isotopes as radiation sources.

LITERATURE CITED

1. Methods of Determining the Economic Efficiency of New Methods, Mechanization and Automation of Industrial Processes [in Russian], Moscow, Izd-vo AN SSSR (1962).
2. Methods of Determining the Economic Efficiency of the Use of Atomic Energy in Agriculture [in Russian], Moscow, Gosatomizdat (1963).
3. A. V. Babergal', V. I. Sinitsyn, and N. I. Leshchinskii, Isotope Gamma-Ray Plants [in Russian], Moscow, Gosatomizdat (1960).

OBTAINING ACCELERATED MONOKINETIC BUNCHES OF ELECTRONS WITH HIGH CAPTURE PERCENTAGE IN A RESONATOR BUNCHER

(UDC 621.384.62)

B. A. Snedkov

Translated from Atomnaya Énergiya, Vol. 19, No. 3,
p. 287, September, 1965
Original article submitted April 6, 1964; in revised form June 15, 1965

Monokinetic bunches of electrons can be accelerated in a system consisting of two resonators, a modulating resonator and an accelerating resonator. Electrons, injected by a continuous-current gun, are velocity-modulated in the gap of the first resonator, and are then grouped into bunches in the drift space at the entry to the second (accelerator) resonator. In the latter the total energy of the bunches is increased and its scatter leveled up, by means of modulation (see figure). The total bunch energy is increased,

$$u = u_0 + u_1 \sin\theta,$$

while the condition for leveling up of the energy scatter of the particles follows from the equality of the derivatives on the energy-distribution phase diagram (see figure):

$$\frac{du}{d\tau_1} = \frac{du_1}{d\tau_1}.$$

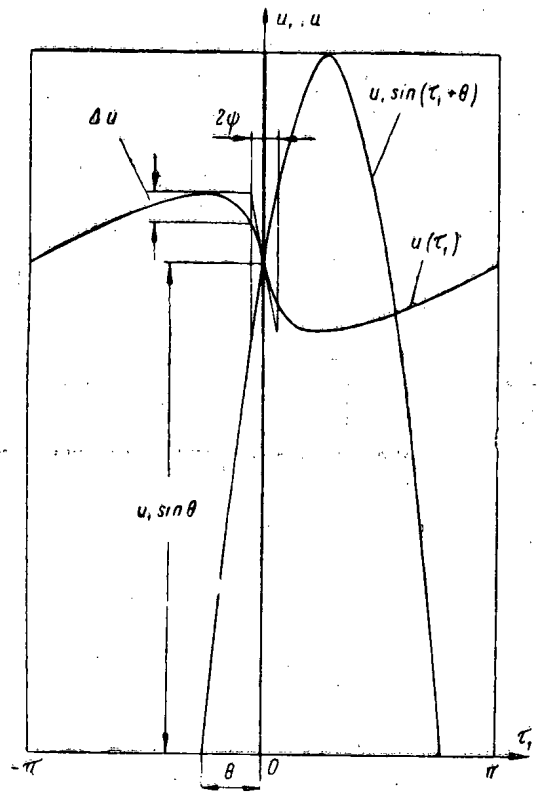

Energy leveling and acceleration of particles in bunch in accelerating resonator. θ phase of accelerating field; τ_1 phase of electrons in gap of accelerating resonator; ψ extent of bunch; Δu residual scatter of particle energy.

The residual energy scatter of the accelerated bunch is due to incomplete matching of the sections of the phase diagrams for $u(\tau_1)$ and $u_1(\tau_1)$ in the phase regions of maximum particle accumulation, i.e., near $\tau_1 \approx 0$. It is convenient to consider a bunch containing not more than 33% captured particles (angle of capture 120°). The particles in such an accelerated bunch have nearly unique energy.

To increase the number of particles in the bunch, some additional modulating resonators must be fitted between the modulating and accelerating resonators. The voltage amplitude at the modulating resonators increases considerably from the former to the latter. The weakly modulated partially bunched electron current in the former is strongly modulated in the latter. The phase diagram of a bunch which has traversed several resonators is similar to $u(\tau_1)$ (see diagram), but its energy scatter is greater and the length of the bunch also rises somewhat. The residual scatter in the accelerated bunch is also somewhat increased, and it is therefore undesirable to include more than three modulating resonators.

A system of three modulating and one accelerating resonator is able to pull up to 70% of all the injected particles into a bunch and to secure less than 0.5% residual energy scatter at the exit of the accelerating resonator.

Over a certain range of current densities, the space charge makes it possible to improve the energy uniformity of the bunches. The relative energy scatter can be reduced to 0.1%.

As well as the dose attenuation, we found the angular distribution of the scattered neutron energy. As in the case of gamma quanta, there is an exponential decrease of the energy flux with increase of the angle θ subtended from the direction of motion of the primary neutrons:

$$J(\theta) = Ae^{-\theta/\theta_0},$$

where θ_0 is the angular distribution constant, A the pre-exponential factor. However, unlike gamma quanta, neutrons display a rather marked dependence of θ_0 on the thickness of the shielding barrier (Fig. 2).

LITERATURE CITED

1. L. M. Shirkin, Atomnaya Énergiya, 17, 509 (1964).
2. G. Gol'dshtein, Principles of Reactor Shielding [in Russian], Moscow, Gosatomizdat (1961).

All abbreviations of periodicals in the above bibliography are letter-by-letter transliterations of the abbreviations as given in the original Russian journal. *Some or all of this periodical literature may well be available in English translation.* A complete list of the cover-to-cover English translations appears at the back of this issue.

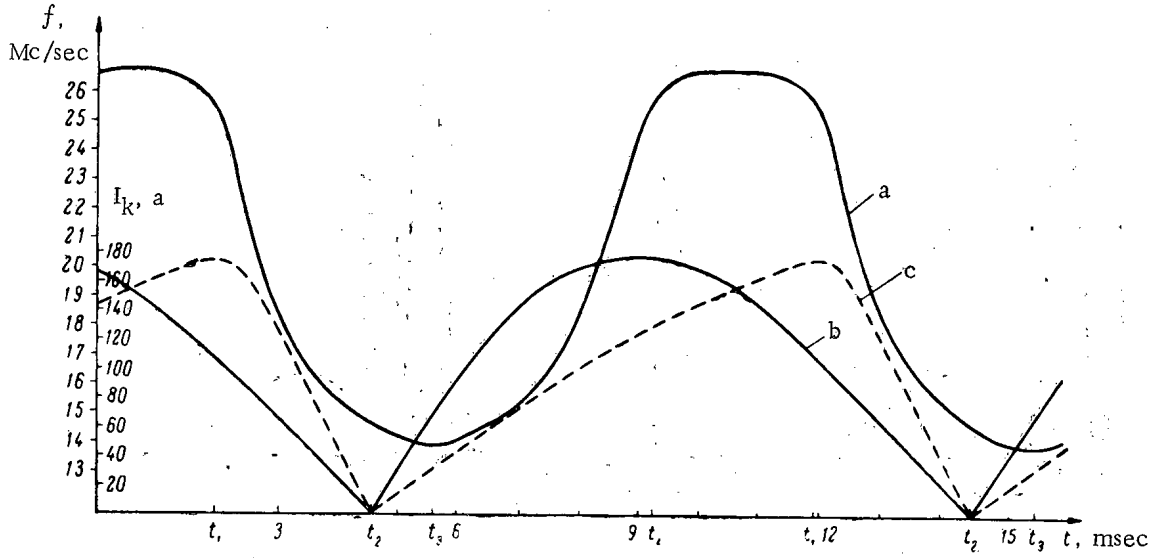

Fig. 2. Time dependences of frequency of accelerating voltage (curve a) and current in stretching coils (curves b and c). t_1 initial time; t_2 time of switching in stretching coils; t_3 end of acceleration; t_4 end of beam stretching.

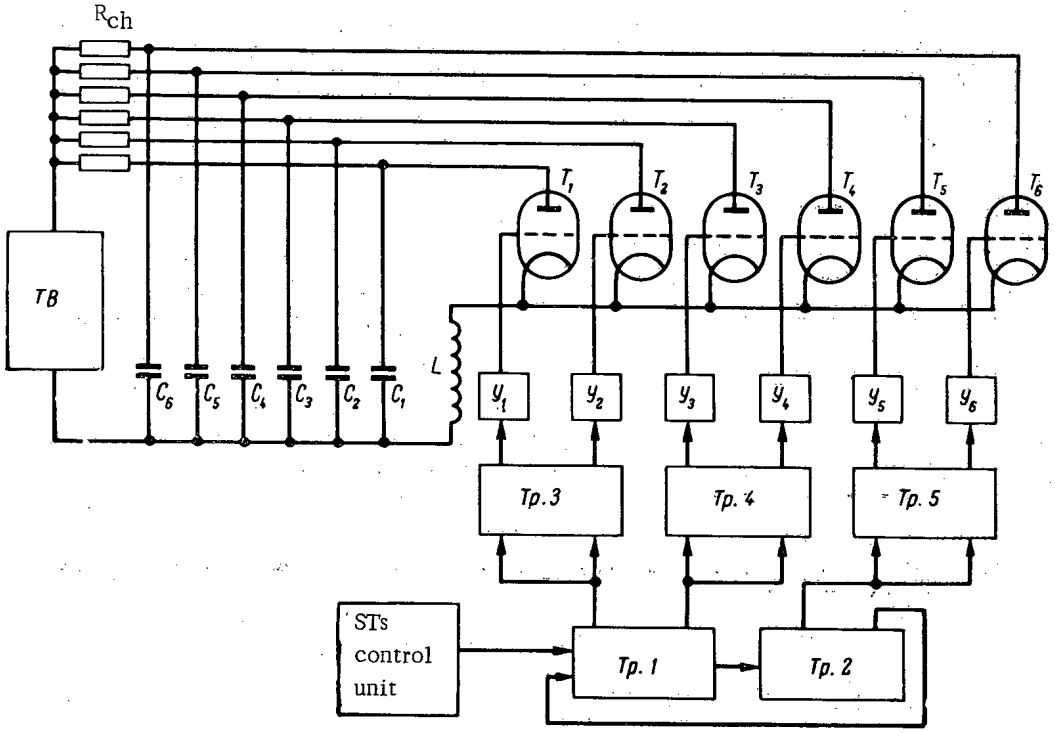

Fig. 3. Control and power supply circuits for stretching coils. TB thyratron rectifier; Tp) trigger; Y) amplifier; T) thyratron; C) capacitor; R_{ch}) charging resistance.

$$\dot{r}_s = \frac{r_s}{1-n} \cdot \frac{1}{E_s \beta_s^2} \cdot \frac{\omega_s}{2\pi} e_0 V_0 \sin \varphi_s = \frac{r_s}{1-n} \cdot \frac{1}{K_s \beta_s^2 \omega_s} \cdot \frac{d\omega}{dt};$$

$\rho_{B.M}(t)$ is the rate of displacement of the equilibrium orbit in azimuth φ_M due to excitation of the first harmonic of the magnetic field;

$$n = -\frac{r}{H} \cdot \frac{\partial H}{\partial r}; \; K = 1 + \frac{n}{1-n} \cdot \frac{1}{\beta^2}; \; \beta = \frac{v}{c};$$

$$\varrho = \frac{R_0}{2} \sum_{l=0}^{\infty} \left\{ \frac{\cos\left[\left(l+\frac{\Omega}{\omega}\right)\varphi+\alpha_l\right]}{\left(l+\frac{\Omega}{\omega}\right)^2-(1-n)} - \frac{\cos\left[\left(l-\frac{\Omega}{\omega}\right)\varphi+\alpha_l\right]}{\left(l-\frac{\Omega}{\omega}\right)^2-(1-n)} \right\} \tag{3}$$

Here Ω is the frequency of the exciting magnetic field, R_0 the radius of the equlibrium orbit.

From Eq. (3) it follows that the only important harmonic is the first, and to a first approximation we can write

$$\varrho = \frac{R_0 h_1}{2n} \sin\frac{\Omega}{\omega}\varphi \sin(\varphi+\alpha_1) = \frac{R_0 h_1}{2n} \sin\Omega t \sin(\omega t+\alpha_1), \tag{4}$$

i.e., the amplitude of forced vibration changes with time in accordance with changes in the exciting magnetic field.

In the region of the final radii (225-275 cm) the exciting magnetic field was created by two coils (Fig. 1, position 7) located on the azimuth of the target symmetrically with respect to its central plane. In the region of 20 cm radius the exciting field was uniform within 10%. In these conditions, to obtain maximum amplitude of the forced vibrations, 10 cm ($\rho_B - \rho_b + 2\rho_c$), a field pulse with maximum intensity 700 oersted is required.

The maximum beam length is determined by the condition that the discharge current pulse cannot be longer than the modulation period, and with a sine pulse is about half the modulation period (Fig. 2).

The coils are excited by discharging a battery of capacitors through a controlled rectifier once in each acceleration cycle. To improve the reliability of the power supply to the coils and reduce the peak value of the discharge current, six discharge units are used. Their sequence of operation is controlled by a control unit with two triggers in series which convert the input synchronization pulses into three and shift them by a modulation period. The converted pulses are fed to the input of three triggers which divide the pulses into two and shift them by three modulation periods at each output (Fig. 3). The trigger pulses coincide with pulses which lock the hf-generator at the end of the acceleration cycle. To increase the pulse length to a value greater than half the modulation period, a sawtooth current pulse must be used in the coils (curve c in Fig. 2). A supply circuit of this type is now being built.

Figure 4 gives the pulse shapes of the meson beams obtained with and without coils.

The length of the stretched beam current pulse is 2.0-2.5 msec at the 0.5 level. Figure 5 plots the intensity of the stretched beam versus the coil current. Part of the beam (15-30% of the intensity) falls on the target before the accelerating voltage is switched off and before the stretching coils are switched in. From these diagrams it is seen, first, that the entire length of the meson beam pulse is about half the length of the coil current pulse; secondly, that with correct choice of the time at which the accelerating voltage is switched in, of the position of the target relative to the coils and of the current in the coils, there is no loss of intensity.

LITERATURE CITED

1. V. I. Danilov et al., B-1-1543, Dubna, OIYaI (1963).
2. B. Hedin, Report, CERN, 61-21 (1961).
3. A. Cabrespine, Compt. Rend., 250, 2224 (1960); A. Cabrespine, J. Phys. Radium, 21, 332 (1960).
4. A. L. Mints and N. K. Kaminskii, Zh. tekhn. fiz., XXVII, 1337 (1957).
5. F. Russel, Nature, 190, 4773 (1961).
6. G. Huxtable, P. Rogers, and F. Russel, Nucl. Instrum. and Methods, 23, 357 (1963).
7. E. H. Molthen, Nucl. Instrum. and Methods, 29, 29 (1964).

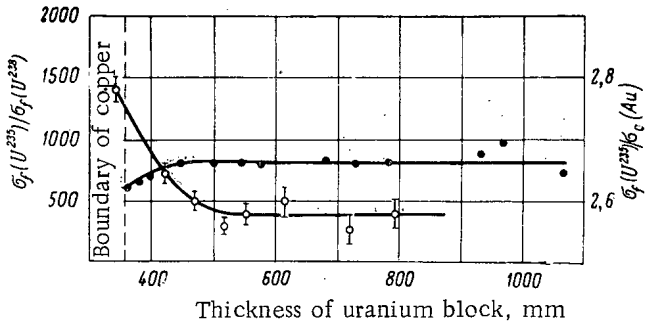

Ratio of reaction cross sections. ●) Ratio of fission cross section of U^{235} to capture cross section of gold; ○) ratio of fission cross section of U^{235} to fission cross section of U^{238}.

We have studied the propagation in improvished uranium metal of neutrons moderated in large thicknesses of copper. Neutrons from the copper reflector of the BR-1 fast-neutron reactor were allowed to fall on a block of uranium metal. The capture cross sections for various elements were determined for the neutron spectrum established in the uranium. We made the measurements, in a cavity in the uranium block, by the activation method and by transmission in spherical geometry.

The figure plots the ratios of fission and capture cross sections measured with miniature fission chambers and gold foil in uranium blocks of various thicknesses. The integral characteristics were different for the various spectra:

$$\frac{\sigma_f(U^{235})}{\sigma_f(U^{238})} = 376 \pm 25 \text{ and } \frac{\sigma_f(U^{235})}{\sigma_c(Au^{197})} = 2.74 \pm 0.12.$$

The considerably lower value of $[\sigma_f(U^{235})]/[\sigma_c(Au^{197})]$ shows that the neutron spectrum formed in this case is much softer.

The table gives capture cross sections for various elements, measured relative to the fission cross section of Pu^{239}. For comparison, it also gives capture cross sections, measured by the same method, for the neutron spectrum established in the uranium reflector of a BR-2 reactor at a distance of 200 mm from the edge of the core [4]. With such uranium thicknesses, the neutron spectrum is nearly asymptotic as regards the constancy of the ratio $[\sigma_f(U^{235})]/[\sigma_c(Au^{197})]$. The last column gives measurements of transmission in spherical geometry. The specimens were spherical layers of gold and iodine of thickness 1 cm.

Cross sections for the asymptotic spectrum in the uranium reflector, calculated with a 26-group system of constants [5], agree with the experimental data.

When a similar calculation was made in the P_3 approximation for the system copper-uranium, there was some softening of the neutron spectrum, but it proved impossible to obtain satisfactory agreement with experiment. This also shows that account must be taken of the effect due to the propagation of inter-resonance-energy neutrons in the uranium.

In the general case, the spectrum established in metallic uranium appears to depend (at least, for practical thicknesses) on the neutron spectrum of the source. It is also noteworthy that the criterion of establishment of an asymptotic spectrum with definite characteristics – constancy of the ratio $[\sigma_f(U^{235})]/[\sigma_f(U^{238})]$ – cannot be regarded as definitive, as this ratio is sensitive to the hard part of the spectrum.

In conclusion the authors would like to thank M. N. Nikolaev for helpful discussion, and the staff of the BR-1 reactor for help with the work.

LITERATURE CITED

1. A. I. Leipunskii et al., Atomnaya Énergiya, 5, 277 (1958).
2. F. Bayer et al., In: Experimental Reactors and Reactor Physics: Proceedings of International Conference on the Peaceful Uses of Atomic Energy (Geneva, 1955), Reports of foreign [non-Soviet] scientists [in Russian], Moscow, Gostekhteorizdat (1956), p. 467.
3. H. Bethe, J. Bejster, and R. Garter, J. Nucl. Energy, 3, 207 (1956).
4. A. I. Leipunskii et al., In: Proceedings of Second International Conference on the Peaceful Uses of Atomic Energy, Reports of Soviet Scientists [in Russian], T. 1, Moscow, Atomizdat (1959), p. 316.
5. L. P. Abagyan et al., Grouped Constants for Calculations on Nuclear Reactors [in Russian], Moscow, Atomizdat (1964).

Absorption Resonance Integrals, barn

Element	R_γ (1/v)	R_γ above 1/v	R_γ (total)	[4]	[5]	[6]	[7]
V	2,2	0,25±0,03	2,45±0,03	—	—	3,3±0,8	2,2
Zr	0,081	1,0±0,2	1,1±0,2	0,7±0,1	2,3±0,5	3,7±0,5	3
Zr^{90}	0,044	0,16±0,02	0,2±0,03	—	—	—	—
Zr^{91}	0,66	6,7±0,8	7,3±0,8	—	—	—	—
Zr^{94}	0,035	0,2±0,03	0,23±0,03	—	—	—	—

true structure of the cross section's energy dependence for nuclei with few levels. However, from the graphs of $\sigma(n, \gamma)$ versus E, it was possible to get accurate values of the integral capture cross section for any reasonably wide energy range.

The cross section for vanadium was absolutely normalized from the capture cross section for thermal neutrons (5.0 ± 0.01 barn); those for zirconium, Zr^{90}, Zr^{91}, and Zr^{94} were normalized from the resonance levels of molybdenum and tungsten. In calculating the normalization coefficient for zirconium with E > 1, account was taken of the variation in efficiency of recording the act of capture with the energy of the indicent neutron, following [9]. The gamma-ray detectors were proportional and scintillation counters.

Results of Measurements

Figures 1 and 2 and the table give the capture cross sections and resonance absorption integrals.

Vanadium. (See Fig. 1.) At 167 eV we find a resonance belonging to V^{50}. Analysis of the area under the peak gives a radiation width Γ_γ = 0.6 ± 0.08 eV. The small peak at 45 eV can be explained by the presence of molybdenum as impurity (0.1 at. %). The known V^{51} resonances at E > 4 keV obey the condition $\Gamma_n >> \Gamma_\lambda$ [11]. Hence, from the relation

$$\sum_{i=1}^{n} R_\gamma = k\bar{\Gamma}_\gamma \cdot \sum_{i=1}^{n} \left(\frac{1}{E_a^i}\right)^2,$$

in which the sum of the resonance integrals is determined from the experimental area under the cross section curve, we can get the value

$$\bar{\Gamma}_\gamma \leqslant 0.75 \pm 0.1 \text{ eV}.$$

The inequality sign applies when there are narrow resonances not disclosed in the total cross sections.

Zirconium. The measurements were made with three types of specimen. In all the specimens, including the separated isotopes, hafnium resonances appeared in the low-energy region. The hafnium contents, calculated from the areas under the peaks, were 0.01-0.6 at. %. It was estimated that these amounts of hafnium would not affect the results above 150 eV.

Zr^{91}. (See Fig. 2.) For groups of levels with energies 180-450 eV with known neutron widths Γ_n, the value

$$\bar{\Gamma}_\gamma = 0.23 \pm 0.03 \text{ eV}.$$

has been obtained [12]. Analysis of the areas under the cross section curve at 500-1000 eV shows that, besides the known level at 685 eV [12], there is a Zr^{91} resonance with E > 685 eV. If we ascribe the area, left after subtracting the contribution of the 685 eV level, to an unidentified resonance at 880 eV [12], we get $\sigma_0 \Gamma_\gamma$ = 69 barn · eV. Hence, with Γ_γ = 0.23 eV, we shall find a corrected width of $\Gamma_n^0 \approx 2 \cdot 10^{-3}$, which is less by a factor of about 35 than the value, $\bar{\Gamma}_n^0$ = 0.07 eV, found for the known resonances with l = 0 [12]. Perhaps the resonance at 880 eV is due to capture of neutrons with orbital momentum l = 1.

Zr^{90}, Zr^{94}. (cf. Fig. 2.) The capture cross sections for these elements for E > 6 keV decrease as 1/E with the neutron energy. For the 2273 eV level (Zr^{94}) with Γ_n = 0.8 ± 0.1 eV, the value Γ_γ = 0.17 ± 0.04 eV has been found [12].

THE HEAVY-MONATOMIC-GAS MODEL AND THE NONSTATIONARY THERMALIZATION OF NEUTRONS IN LEAD

(UDC 539.125.523.5)

Sh. Kenzhebaev

Translated from Atomnaya Énergiya, Vol. 19, No. 3,
pp. 296-297, September, 1965
Original article submitted November 20, 1965

In the heavy-monatomic-gas model, the appropriate Wilkins equation takes an especially simple form: the integral operators are replaced by simpler differential operators and at the same time satisfy the Principle of Detailed Balancing. Since the model takes no account of chemical bonding or crystalline effects, it does not always yield satisfactory results. The heavy-gas approximation becomes better as a representation of a real moderator as the element gets heavier and the Debye temperature lower. However, when the diffusion parameters of an organic substance such as diphenyl $C_{12}H_{10}$ are measured, the coefficients of diffusive cooling obtained by the pulse method agree with theoretical calculations based on the heavy-monatomic-gas model [1].

In practice, allowance for the chemical bonds leads to hardening of the spectrum. The properties of the model are expressed in the second moment of energy transfer and the thermalization time. In particular, the second transfer is much less in graphite and beryllium, while the thermalization time is several times greater than the values found for free atoms [2-4].

In [5] a pulsed source was used to study the establishment of equilibrium neutron velocities in lead. Lead has a high mass and a low Debye temperature (θ = 88°K). We can thus be confident that neutron scattering in lead is satisfactorily represented by the heavy-monatomic-gas model. It is therefore interesting to calculate the mean neutron velocity in lead in that range of slowing-down times for which the spectrum is close to the equilibrium Maxwell type, and to compare the value thus found with experiment.

In the thermalization-time problem, the neutron density can be written as

$$n(y,\ t)=\sum_k C_k e^{-\alpha_k t} e^{-y^2} y^2 \psi_k(y),$$

where y is the velocity measured as a multiple of $\sqrt{2kT/m}$. The time problem reduces to the following equation for the eigen-functions ψ_k, corresponding to the eigen-values Δ_k:

$$y\frac{d^2\psi_k}{dy^2}+(3-2y^2)\frac{d\psi_k}{dy}-(\Delta_k-4\lambda y)\psi_k=0. \tag{1}$$

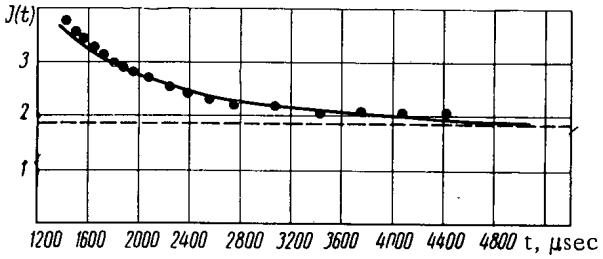

Approximation to equilibrium value of mean neutron velocity in lead.

Here $\lambda=-\frac{1}{2}Ml_s^2\Omega$, $\Delta_k=2Ml_s\left(\frac{1}{T_0}-\alpha_k\right)$; Ω is a geometrical parameter corresponding to the fundamental harmonic, T_0 the mean lifetime of neutrons in lead. Then the mean neutron velocity in the moderator at time t is

$$\overline{y(t)}=\frac{\int_0^\infty n(y,\ t)\,y\,dy}{\int_0^\infty n(y,\ t)\,dy} \tag{2}$$

Equation (1) has been solved numerically for the first three harmonics for the case corresponding to the experi-

THE USE OF A ZIRCONIUM-TRITIUM SOURCE FOR NONDISPERSIVE X-RAY SPECTRAL ANALYSIS

(UDC 539.16.07)

Yu. P. Betin, M. I. Bursukova, V. I. Verkhovskii, and L. S. Shelkov

Translated from Atomnaya Énergiya, Vol. 19, No. 3, pp. 297-298, September, 1965
Original article submitted June 15, 1964; in revised form, April 13, 1965

The spectrum of the electromagnetic radiation emitted by zirconium-tritium sources contains a continuous portion, corresponding to bremsstrahlung with a quantum energy of up to 15 keV, and a line of the characteristic Zirconium L radiation, with a quantum energy of 2.1 keV [1,2]. These properties make it possible to use such sources for exciting the characteristic K x-ray radiation of light and intermediate elements. The use of zirconium-tritium sources for the excitation of K radiation in elements with atomic numbers from Z = 12 (magnesium) to Z = 30 (zinc) has been described in the literature [1, 3-8]. The relative effectiveness of a source when it is used for exciting x-ray fluorescent radiation depends on the atomic numbers of the elements in the irradiated specimen, on the measurement geometry, and on the parameters of the detector used for recording the characteristic radiation.

We measured the relative effectiveness of a zirconium-tritium source for various elements over a wide range of Z, from 16 to 30. To excite the fluorescent radiation we used a standard "thick" zirconium-tritium target with an activity of about 12 Ci on a tungsten backing. The diameter of the active surface of the target was 15 mm. The thickness of the zirconium layer was 16 mg/cm^2. The radiation spectrum of such a target is given in [2].

Figure 1 shows the relative positions of the zirconium-tritium target, the specimen, and the proportional counter. To measure the intensity of the x-ray fluorescent radiation excited in the specimens, we used a proportional counter with a beryllium side window measuring 8 × 30 mm and 0.2 mm thick, filled with a mixture of xenon and isopentane to a pressure of about 500 mm Hg [9].

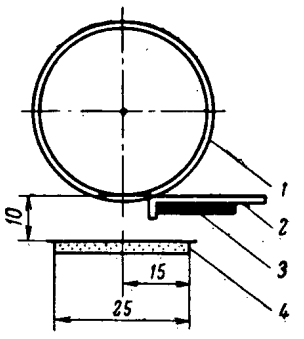

Fig. 1. Arrangement of the zirconium-tritium source, the specimen, and the proportional counter: 1) counter; 2) screen (aluminum, 1.5 mm thick); 3) zirconium-tritium target; 4) specimen.

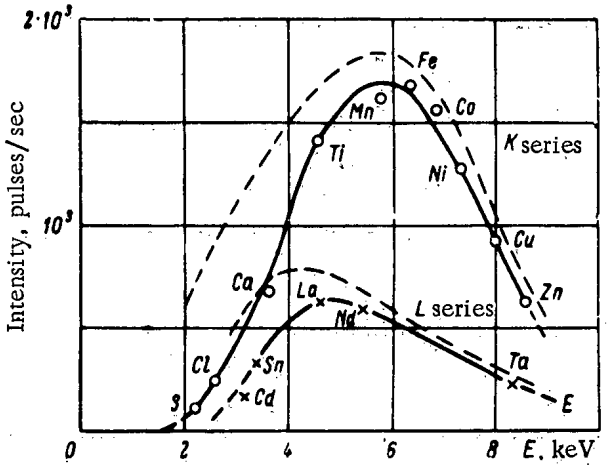

Fig. 2. Intensity of K and L radiations as a function of the energy of the characteristic-radiation quanta (dashed curves show the data after correction for the efficiency of the detector).

FREEING SODIUM FROM THE PRODUCTS OF ITS REACTION WITH WATER IN A CIRCULATION LOOP

(UDC 621.039.534.6)

V. I. Subbotin, P. L. Kirillov, F. A. Kozlov,
N. N. Ivanovskii, and V. M. Makarov

Translated from Atomnaya Énergiya, Vol. 19, No. 3,
pp. 298-300, September, 1965
Original article submitted March 1, 1965

In high-power nuclear power stations there are prospects for the use of sodium-water steam generators with a single heat-transfer wall. This method is cheaper and simpler to construct than conventional types. However, in this type of steam generator there is an increased risk of water coming into contact with the sodium. Since the water in the steam generator is at higher pressure than the sodium, leaks in the steam generator may allow considerable amounts of water to get into the sodium circuit. An important problem is thus to purify the sodium from the products of its reaction with water.

In [1] it is shown, by the methods of chemical thermodynamics, that when excess sodium reacts with water the equilibrium products formed are sodium oxide and hydride:

$$4Na + H_2O \longrightarrow Na_2O + 2NaH. \quad (1)$$

We should therefore expect that purification of sodium from the products of its reaction with water will involve the recovery of sodium hydride and oxide. There are well-developed methods [2] for freeing sodium from its oxide by means of cold traps. However, there are no reliable data available on the simultaneous purification of sodium from oxide and hydride, or from hydride alone. (The author of [3] discusses the possibility of trapping sodium hydride in cold traps.) Our research therefore comprised two stages: we first studied the purification of sodium from its hydride, then from the products of its reaction with water.

The work was done with an ordinary sodium circulation loop. Measured portions of hydrogen or water were fed into the gas space of the tank pump. To avoid precipitation of oxide or hydride on the walls of the tank's gas space, the temperature in the latter was kept 50-70° higher than the temperature of the sodium. The operation of the cold trap was monitored by means of the plug indicator described in [2, 3].

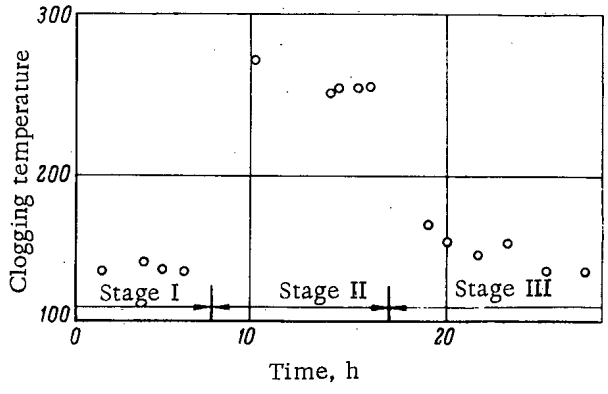

Fig. 1. Purification of sodium from hydrogen. Stage I: filtration through cold trap; Stage II: Cold trap switched off, 2.2 g hydrogen fed into pump tank; Stage III: filtration through cold trap.

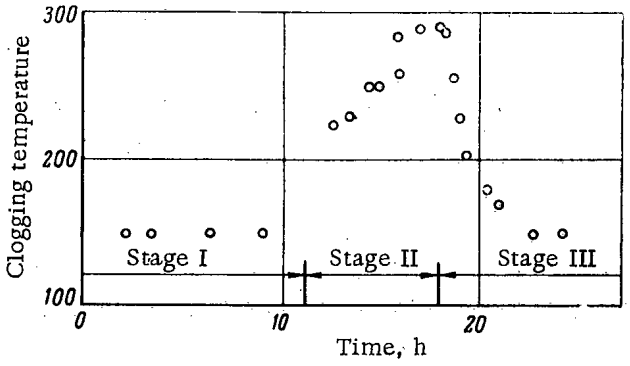

Fig. 2. Purification of sodium from the products of its reaction with water. Stage I: filtration through cold trap; Stage II: cold trap switched off, 105 g water added; Stage III: filtration through cold trap.

THERMAL CONDUCTIVITY OF HELIUM AT TEMPERATURES OF 0-1000°C AND PRESSURES OF 1-200 ATM

(UDC 621.039.534.3)

N. B. Vargaftik and N. Kh. Zimina

Translated from Atomnaya Énergiya, Vol. 19, No. 3,
pp. 300-303, September, 1965
Original article submitted December 21, 1964; in revised form, May 14, 1965

A number of studies published in recent years have been concerned with the thermal conductivity λ of helium over a wide range of temperatures and pressures [1-7]. However, the results of experiments conducted by various authors are not in sufficiently good agreement, and this makes it difficult to determine the behavior of the function $\lambda = f(t, p)$.

The purpose of the present study is the experimental investigation of the thermal conductivity of helium in the 0-1000°C temperature range at a pressure of 1 atm, as well as an analysis of published experimental data on the thermal conductivity of this gas at various values of t and p. The investigations were conducted on the apparatus described in [8], using the hot-wire method. (The methods ued for the calculations and for processing the experimental data are described in the same reference.)

In the processing of the experimental data, it is particularly important to make a correction for the temperature jump, since at high temperatures the value of the correction for helium is considerable, even at p = 1 atm, as will be shown below.

As is known [9], the correction for the temperature jump is calculated by means of the formula

$$\Delta t = \Delta t_{gas} + B\left(\frac{1}{p}\right), \tag{1}$$

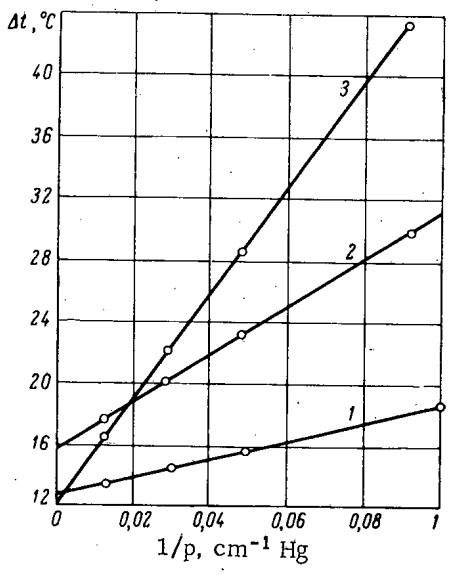

Fig. 1. Graph of $\Delta t = f(1/p)$ for various values of temperature: 1) 355°C; 2) 652°C; 3) 962°C.

where Δt is the measured temperature drop between the wire and the inner surface of the measuring-tube wall; Δt_{gas} is the actual temperature drop in the gas layer; B is a value dependent on the physical properties of the gas and the wire material, as well as on the geometry of the instrument and the total amount of heat, Q, generated by the wire.

Thus, Δt must be linear function of 1/p when Q = const. From the measured values of Δt corresponding to different pressures at the same average gas temperature, we can construct the linear function $\Delta t = f(1/p)$. By extrapolating Δt to the value 1/p = 0, we can find the value of Δt_{gas} which appears in the basic formula for determining the thermal conductivity λ of a gas by the hot-wire method:

$$\lambda = A\frac{Q}{\Delta t_{gas}}, \tag{2}$$

where A is a constant depending on the instrument. For a given gas pressure and specified conditions of temperature and instrument geometry, the temperature-jump correction Δt_j can be found by the formula

$$(\delta t_j)_p = \frac{\Delta t_p - \Delta t_{gas}}{\Delta t_p}, \tag{3}$$

where the subscript p represents the gas pressure for which the correction is determined.

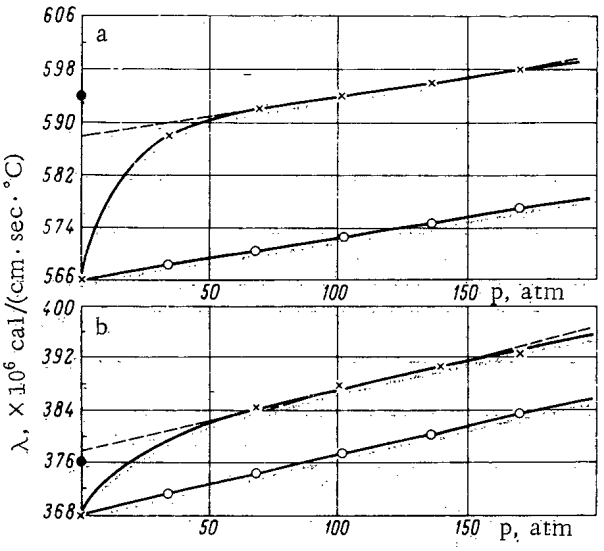

Fig. 3. Comparison of the experimental data of [6] with the results obtained by Enskog's theoretical formula for temperatures of 315.6°C (a) and 37.8°C (b): ○) calculation by Eq. (5) for values of λ_0 taken from [6]; ×) experimental data of [6]; ●) value of λ obtained by correcting for the temperature jump; ———) Enskog's calculation for high pressures and extrapolation of λ to p = 0.

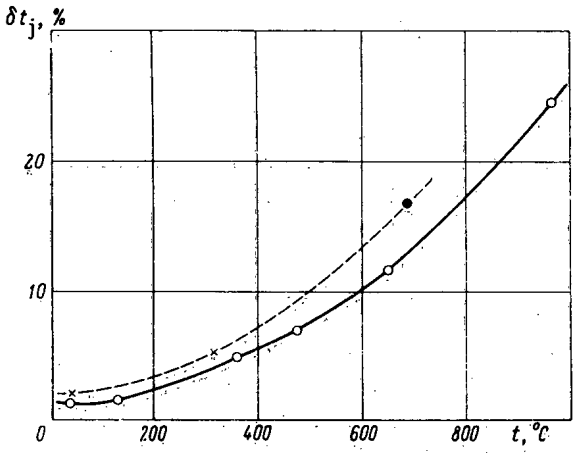

Fig. 4. Graphs of $\delta t_j = f(t)$ obtained in the present study and in [6]: ○) experimental data of the present study; ●) recomputation using the data of [12]; ×) values of δt_j obtained from the 37.8°C and 315.6°C isotherms [6]; ———) assumed graph for [6].

Enskog's formula for t = 37.8°C and t = 315.6°C. Figure 3 indicates that the differences between experimental and calculated data increase with increasing pressure along the initial part of the curve but remain constant at higher pressures.

The reasons for the difference between the experimental results and the Enskog theory, which was worked out approximately for a monatomic gas, were not given in [6]. However, [6] took no account of the correction for the temperature jump between the gas and the surfaces of the coaxial cylinders, which was quite large for light gases, even when p > 1 atm.

Our experiments, conducted at various pressures, enabled us to determine the value of the correction for the temperature jump between the helium and the platinum. In the apparatus used by Johannin, Wilson, and Vodar [6] the cylinders were made of silver. Naturally, the magnitude of the temperature jump depends on the relationship between the atomic (molecular) weights of the gas and the solid. However, there has been little investigation of this question from the quantitative viewpoint. We therefore used the results of Rothman's experiments [12] on the temperature jump between helium and silver cylinders, which were obtained only for t = 686°C. The gap in this apparatus measured 0.6 mm. At this temperature and with p = 1 atm, it was found that

$$(\delta t_j)_p = \frac{(\Delta t_p - \Delta t_{gas}) \cdot 100\%}{\Delta t_p} = \frac{(2.22 - 2.10) \cdot 100\%}{2.22} = 5.4\%,$$

where the subscript p corresponds to 1 atm. For coaxial cylinders (with the same cylinder material and the same values of δt_j is inversely proportional to the magnitude of the gap [12]:

$$\frac{(\delta t_j)_1}{(\delta t_j)_2} = \frac{\delta_2}{\delta_1} \quad (6)$$

Consequently, for the apparatus described in [6], where t = 686°C and p = 1 atm, we have δt_j = 16.2%, since δ = 0.2 mm in the apparatus used by the French authors and δ = 0.6 mm in Rothman's apparatus.

Figure 4 shows the graph of $\delta t_j = f(t)$ for p = 1 atm, plotted from experiments on thermal conductivity of helium performed on the apparatus we used. It follows from this graph that δt_j = 12% when t = 686°C. Thus, on the ap-

3. W. Leidenfrost, Intern. J. Heat and Mass Transfer, 7, No. 4 (1964).
4. E. Commings and J. Lenoir, Chem. Eng. Prog., 47, 223 (1951).
5. N. V. Tsederberg, V. N. Popov and N. A. Morozova, Thermophysical Properties of Helium [in Russian], Moscow – Leningrad, Gosénergoizdat (1961), p. 45.
6. P. Johannin, M. Wilson, and B. Vodar, Second Symposium on Thermophysical Properties, sponsored by ASME, January 24-26, 1962, Academic Press (New York, 1962), p. 418.
7. N. Blais and J. Mann, J. Chem. Phys., 32, 1459 (1960).
8. N. B. Vargaftik and N. Kh. Zimina, Teplofizika Vysokikh Temperatur, 2, 716 (1964).
9. D. L. Timpot and N. B. Vargaftik, Izv. Vsesoyuz. teplotekhn. in-ta, No. 9, 1 (1935).
10. J. Hirschfelder, C. Curtiss, and R. Bird, Molecular Theory of Gases and Liquids [Russian translation], Moscow, Izd-vo inostr. lit. (1961), p. 497.
11. M. Wilson, Jr., O. T. S. Dept. of Comm. Ga 1355 (January, 1960).
12. A. Rothman, Thermal Conductivity of Gases at High Temperatures. United States Atomic Energy Commission (January, 1954).

All abbreviations of periodicals in the above bibliography are letter-by-letter transliterations of the abbreviations as given in the original Russian journal. *Some or all of this periodical literature may well be available in English translation.* A complete list of the cover-to-cover English translations appears at the back of this issue.

TABLE 1. Chemical Composition and Certain Shielding Parameters of Materials

Number	Material	Density, kg/m³	Oxygen and hydrogen content of water, kg/m³		Other elements, kg/m³										High energy neutrons and gamma rays		Fast neutrons on the fission spectrum Σ_{rem}, $\times 10^3$	Thermal neutrons	
			H	O	B	C	O	Mg	Al	Si	S	K	Ca	Fe	Σ_{in}‡, $\times 10^4$	χ, $\times 10^3$		Σ_a, $\times 10^3$	Σ_s, $\times 10^2$
1	Water	1000	111	889	—	—	—	—	—	—	—	—	—	—	14,3	1,64	9,96	2,19	26,95
2	Sinter cakes and ore-melt crusts	1900	—	—	260	19	948	278	125	22	—	—	249	—	—	—	2,84	1010	1
3	Boron mud	2170	39	308	31	—	745	—	22	340	—	—	577	108	—	—	3,12	61	5,5
4	Gypsum	2300	52	420	—	—	856	—	—	431	—	—	538	—	10,1	1,99	4,40	0,77	6,5
5	MNB brand boron chamotte	2370	1	10	113	—	1282	21	558	328	2	—	39	16	—	—	3,56	199	1,22
6	MB brand boron chamotte	2370	—	—	79	—	1128	7	536	570	—	—	10	40	—	—	3,44	140	1,40
7	Ordinary chamotte	2390	—	—	—	—	1250	4	362	720	4	—	12	33	9,4	1,95	3,26	0,21	1,06
8	Limestone	2400	—	—	—	253	1175	14	11	22	3	—	909	10	9,2	2,03	3,16	0,31	1,72
9	Andesite	2500	2	20	—	—	1175	186	265	690	—	21	—	140	9,33	1,99	3,08	0,34	1,26
10	Marble	2500	4	33	—	301	1199	30	—	—	—	—	946	11	9,27	2,04	3,26	0,29	1,98
11	Granite	2500	8	64	—	—	1176	33	127	783	13	—	139	156	9,34	2,02	3,28	0,39	1,10
12	Calcium borate	2500	72	578	306	—	848	—	—	35	—	—	628	32	—	—	5,10	513	8,10
13	Boron carbide	2519	—	—	2172	347	—	—	—	—	—	—	—	—	—	—	5,20	3612	2,05
14	Calemanite	2560	76	638	364	—	988	—	—	—	—	—	493	—	—	—	5,32	596	8,40
15	Magnesian cement	2580	39	312	—	—	893	1195	33	31	6	—	69	—	10,2	1,87	3,99	0,40	4,70
16	Quartz sand	2600	—	—	—	—	1382	—	27	1173	18	—	—	—	9,4	1,94	3,18	0,138	1,01
17	Serpentine	2620	32	256	—	—	1085	630	—	556	4	—	57	—	9,97	1,89	3,86	0,354	3,94
18	Datolite	2790	38	304	113	—	1103	16	68	438	—	—	658	52	—	—	3,94	170	4,61
19	Gypsum alumina cement	2920	18	147	—	—	1146	12	422	140	72	—	885	75	9,26	2,12	3,34	0,50	2,65
20	Boron cement	2950	5	43	34	—	946	38	88	341	18	—	1375	62	—	—	2,88	48,7	1,64
21	Alumina cement	3000	—	—	—	—	1146	20	580	124	26	—	968	134	8,89	2,17	2,89	0,45	1,16
22	Diabase	3000	2	20	—	—	1322	210	270	685	—	15	171	304	9,16	1,99	3,09	0,45	1,15
23	Basalt	3000	2	20	—	—	1369	183	291	758	—	36	214	126	9,25	2,02	3,13	0,34	1,08
24	Portland cement	3080	3	27	—	—	1129	34	68	395	31	—	1309	82	8,83	1,95	2,78	0,43	1,50
25	Limonite	3120	36	288	—	—	888	6	74	255	—	—	16	1557	8,88	2,4	3,46	1,68	3,89
26	Chromite	3520	17	137	—	—	1435	359	264	193	8	—	78	575/453*	9,24	2,2	3,34	1,09	2,21
27	Hematite	3980	—	—	—	—	1305	71	—	210	—	—	72	2320†	8,22	2,51	2,69	1,64	1,30
28	Barytic ore	4200	2	19	—	—	1184	—	—	88	516	—	—	2226/164	7,32	2,85	2,33	0,50	0,84
29	Scrap metal	4700	—	—	—	—	1466	19	—	102	—	—	16	3095	8,08	2,57	2,43	2,30	1,30
30	Steel	7800	—	—	—	—	—	—	—	—	—	—	—	7800	7,10	3	2,14	2,70	1,20

* Chromium content.

† Barium content.

‡ For $E_n \geq 100$ MeV

Declassified and Approved For Release 2013/03/15 : CIA-RDP10-02196R000700020003-3

TABLE 4. Composition of Concretes

Initial density, kg/m³	Total amount of water, kg*	No. of materials taken from Table 1	Mixing water, % of concrete density	Amounts of materials, % by wt. of concrete denisty	Boron content of concrete, kg	Iron content of concrete, kg
2000	253	24+6+5	12,5	15,7+67,1+4,7	43,3	31,6
2000	253	24+6+5	12,5	15,7+54,0+17,8	59,7	13,7
2050	295	20+5	13,9	19,0+67,1	70,5	17,6
2150	429	24+17	11,3	10,7+78,0	—	6,1
2170	564	24+4	10,8	14,0+75,2	—	9,3
2320	298	24+7+13+27	12,6	12,9+47,7+1,0+25,8	20,7	372,4
2330	430	24+17+27	13,0	13,0+47,7+26,3	—	363,1
2340	430	24+7+26+17	12,6	12,8+12,8+26,0+35,8	—	89,9
2350	134	24+16+8	5,6	9,4+28,9+56,1	—	11,6
2390	206	24+13+16+8	8,6	12,3+3,4+28,6+47,1	70,8	12,3
2390	208	24+13+16+8	8,6	12,3+1,7+30,3+47,1	35,4	12,3
2390	291	24+12+16+8	10,5	8,4+6,2+27,2+47,5	18,0	12,1
2400	212	21+16+8	8,8	12,7+25,8+52,7	—	19,0
2400	250	24+16+8	10,4	18,7+18,8+52,1	—	17,3
2400	354	24+3+16+8	12,8	6,1+12,1+17,5+51,5	4,1	23,1
2420	401	24+7+27+17	12,4	12,7+12,7+25,7+36,5	—	374,4
2430	510	24+18	12,2	17,5+70,3	69,0	43,1
2700	478	24+25	8,9	11,1+80,0	—	1074,0
2770	406	24+4+27	6,5	12,7+39,2+41,6	—	684,3
3270	186	24+16+27	5,6	9,2+19,2+66,0	—	1275,0
3300	232	24+14+28	5,6	14,7+7,3+72,4	33,6	111,0
3340	208	24+14+27	5,4	11,4+6,6+76,6	30,8	1504,0
3370	312	19+25+27	6,5	8,9+21,4+63,2	—	1623,0
3460	500	24+26	11,3	10,1+78,6	—	387,5
3540	341	19+28	8,5	13,5+78,0	—	120,1
3550	219	24+28	5,6	9,8+84,6	—	119,2
3630	335	15+27	8,5	11,3+80,2	—	1707,0
3660	183	24+27	4,9	8,2+86,9	—	1795,0
4300	183	24+16+27+30	4,2	8,1+9,3+16,3+62,1	—	3087,0
4440	416	19+25+30	5,1	5,0+38,8+51,1	—	3126,0
4650	186	24+16+30	3,9	6,4+10,9+78,8	—	3698,0
4730	356	19+25+30	5,7	6,3+14,0+74,0	—	3837,0
5080	191	24+14+30	3,2	5,3+4,5+87,0	32,2	2921,2
5290	332	19+30	5,7	10,8+83,7	—	4435,0
5350	262	24+30	4,8	10,6+84,6	—	4535,0
6310	133	24+30	2,1	4,6+93,3	—	5890,0

* This includes both the chemically bound water in the materials and the mixing water.

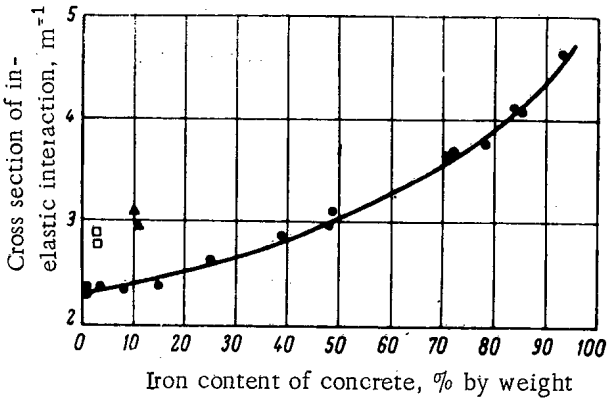

Fig. 2. Variation of the cross section of inelastic interaction of ultra-high-speed neutrons as a function of the iron content of concretes: □) Barytic concrete; ▲) chromite concrete; ●) concretes containing iron ore or steel scrap.

SENSITIVITY OF SCINTILLATION METHOD IN GAMMA-RAY FLAW DETECTION

(UDC 620.179.15)

A. A. Arkhangel'skii and R. Yu. Volkovyskii

Translated from Atomnaya Énergiya, Vol. 19, No. 3,
pp. 308-309, September, 1965
Original article submitted September 14, 1964; in revised form, February 2, 1965

The sensitivity of gamma-ray flaw detection is assessed by the minimum size Δx_{min} of the defects shown up. This quantity is associated with the measurement error: the smaller the latter, the smaller will be Δx_{min} and the higher the sensitivity. The lowest instrumental error is obtained with the scintillation method [1, 2], which has high detector efficiency and sensitivity to radiation and low noise level in the measurement circuit. We shall therefore assume that (at least over a restricted range of thickness of the component under test and of radium gamma-equivalents of the radiation sources) instrumental error is unimportant and the sensitivity is determined purely by the statistical error, i.e., by fluctuations in the number of gamma quanta.

Let us derive a relation for the minimum detectable defect size Δx_{min} in terms of the thickness of the test component and the integral gamma-quantum flux incident on the component, assuming that the sensitivity is determined by the statistical error. Following the experimental method of determining the size of the minimum detectable defect, let us assume that ΔI_{min}, the variation in the gamma-quantum flux due to the defect, is k time greater than ΔI_{fl}, the variation due to fluctuations:

$$\Delta I_{min} = k\Delta I_{fl}. \tag{1}$$

The relative r.m.s. error in measuring the flux, arising through fluctuations in the number of gamma quanta, can [3, 4] be written as

$$\frac{\Delta I_{fl}}{I} = \frac{\eta}{\sqrt{2\tau\nu I}}, \tag{2}$$

where I = flux of gamma quanta incident on scintillator (integral flux), τ = RC = time constant of integrating circuit, ν = detector efficiency, η = amplitude distribution coefficient of current pulses at output of photomultiplier. For the pulse-count method $\eta = 1$.

The change in flux due to a minimum-size defect is given by

$$\Delta I_{min} = \frac{k\eta}{\sqrt{2\tau\nu}}\sqrt{I}. \tag{3}$$

As a rule, a sharply collimated beam of gamma quanta is used in work with the scintillation method; we shall therefore consider a parallel beam traversing the test substance. The change ΔI in flux due to a defect of small dimension Δx can be written

$$\Delta I = I_0 e^{-\mu x}\mu\Delta x, \tag{4}$$

where I_0 is the flux of gamma quanta incident on the component under test (in the conditions of the experiment this may be regarded as proportional to the radium gamma-equivalent of the radiation source). By Eq. (4), the size of the minimum detectable defect is related to the flux change ΔI_{min} by the relation

$$\Delta x_{min} = \frac{\Delta I_{min}}{I_0 e^{-\mu x}\mu}. \tag{5}$$

Substuting for ΔI_{min} in Eq. (5) from Eq. (3), we get

gamma radiation from Co^{60} the theoretical and experimental results agreed for thicknesses 30-150 mm, and for gamma rays from Cs^{137} for thicknesses 20-120 mm. For large thicknesses, the size of the minimum detectable defect increases rapidly, as predicted by Eq. (7). At low thicknesses there is a deviation from Eq. (7), and the minimum detectable defect size is independent of thickness for such thicknesses.

The elementary theory of sensitivity based only on statistical errors is undoubtedly of use. With high-sensitivity measuring equipment and sources with small enough radium gamma-equivalents, instrumental error can be neglected over a certain range of thicknesses, and the formulae given above can be used to determine the sensitivity of gamma-ray flaw-detection.

LITERATURE CITED

1. A. A. Arkhangel'skii and G. D. Latyshev, Zavodsk. Laboratoriya, 23, No. 4, 430 (1957).
2. A. A. Arkhangel'skii and G. D. Latyshev, In: Proceedings of Conference at Tashkent on the Peaceful Uses of Atomic Energy. T. 2., Tashkent, Izd-vo AN UzSSR (1960), p. 47.
3. N. N. Shumilovskii and L. V. Mel'ttser, Principles of the Theory of Automatic Control Systems Using Radioactive Isotopes [in Russian], Moscow, Izd-vo AN SSSR (1959).
4. L. K. Tatochenko, Radioactive Isotopes in Instrument Engineering [in Russian], Moscow, Atomizdat (1960), P. 178.
5. A. A. Arkhangel'skii, "Zhel.-dor. transport," No. 8, 36 (1959).

All abbreviations of periodicals in the above bibliography are letter-by-letter transliterations of the abbreviations as given in the original Russian journal. *Some or all of this periodical literature may well be available in English translation.* A complete list of the cover-to-cover English translations appears at the back of this issue.

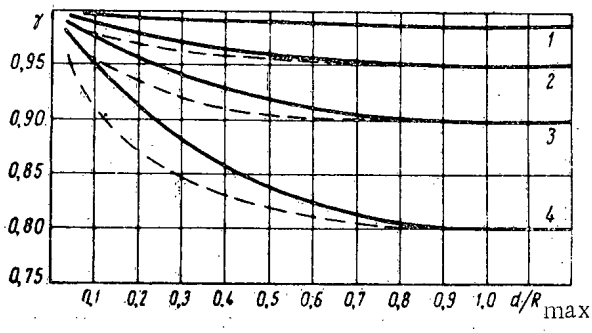

Fig. 2. γ versus dimensions of gas space, coating thickness and range of recoil protons, for various values of a/d: 1) 0.01; 2) 0.05; 3) 0.1; 4) 0.2. ———) Directed neutron flux; - - - - -) isotropic neutron flux.

$$\gamma = \frac{W_{\text{fill}}(a, d)}{W(d)} = 1 - \frac{W_W(d) + W_W(a) - W_W(a+d)}{W(d)}. \quad (3)$$

If a << d,

$$\gamma = 1 - \frac{W_W(a) - aW'_W(a)}{W(d)}. \quad (4)$$

In [5] it was shown that

$$W(d) = \frac{N_p E_n}{2} d$$

and

$$W_W(x) = \begin{cases} W(d) \dfrac{R_{\max}}{\alpha} \alpha \left(1 - 2\alpha + \dfrac{9}{7}\alpha^{4/3}\right) \\ \text{for } \alpha \leqslant 1; \\ W(d) \dfrac{R_{\max}}{d} \cdot \dfrac{2}{7} \text{ for } \alpha \geqslant 1, \end{cases} \quad (5)$$

where $\alpha = (x/R_{max})$; R_{max} = range of protons with maximum energy equal to the neutron energy E_n; N_p = number of knock-on protons produced in unit mass of the substance.

Putting Eq. (5) into Eq. (4) and taking a << d, we get

$$\gamma = \begin{cases} 1 - 4\dfrac{a}{d}\delta\left(1 - \dfrac{3}{4}\delta^{1/3}\right) \text{ for } \delta \leqslant 1; \\ 1 - \dfrac{a}{d} \text{ for } \delta \geqslant 1, \end{cases} \quad (6)$$

where $\delta = (d/R_{max})$. A similar relation can be derived for a chamber situated in an isotropic neutron flux. In this case, as shown in [5],

$$W_W(x) = \begin{cases} W(d) \dfrac{R_{\max}}{d} \alpha \left(1 - \dfrac{1}{2}\alpha - \dfrac{1}{3}\alpha^2 + \alpha \ln \alpha\right) \\ \text{for } \alpha \leqslant 1; \\ W(d) \dfrac{R_{\max}}{d} \cdot \dfrac{1}{6} \text{ for } \alpha \geqslant 1. \end{cases} \quad (7)$$

Calculate as before: then for an isotropic neutron flux we get

$$\gamma = \begin{cases} 1 - \dfrac{a}{d}\delta(\delta - 2\ln\delta) \text{ for } \delta \leqslant 1; \\ 1 - \dfrac{a}{d} \text{ for } \delta \geqslant 1. \end{cases} \quad (8)$$

Figure 2 plots the ratio of the energy evolved in a plane chamber with conducting coating to the energy evolved in a strictly homogeneous chamber, versus the distance between the chamber walls expressed as a multiple of the path of maximum-energy protons.

As an example of the application of the results obtained, let us consider a plane polyethylene chamber filled with ethylene, in a directed flux of neutrons with energy 1 MeV. The distance between the chamber walls is 1 cm, which corresponds to ~1.26 mg/cm². The range of protons with maximum energy 1 MeV is 2.8 mg/cm² [6]. Thus in this case $d/R_{max} = 0.45$. From the curves of Fig. 2 we find that the error in determining the absorbed dose of such a chamber with a conducting coating is equal to:

~15% ($\gamma = 0{,}85$) for $a = 0{,}25$ mg/cm² ($a/d = 0{,}2$);
~8% ($\gamma = 0{,}92$) for $a = 0{,}126$ mg/cm² ($a/d = 0{,}1$);
~4% ($\gamma = 0{,}96$) for $a = 0{,}063$ mg/cm² ($a/d = 0{,}05$);
~1% ($\gamma = 0{,}99$) for $a = 0{,}013$ mg/cm² ($a/d = 0{,}01$).

In the last case the error is below 1%.

MEASUREMENT OF THE EXTERNAL BACKGROUND IRRADIATION OF THE INHABITANTS OF USSR CITIES

(UDC 539.16.04)

I. A. Bochvar, I. B. Keirim-Markus, A. A. Moiseev, T. I. Prosina, and V. V. Yakubik

Translated from Atomnaya Énergiya, Vol. 19, No. 3, pp. 311-312, September, 1965
Original article submitted April 1, 1965

In recent years a great deal of attention has been devoted in many countries to a study of the level of background irradiation caused by natural radioactive isotopes contained in the soil and other components of the external environment and by cosmic rays, as well as to the determination of tissue irradiation doses of the population. The results of the investigations published up to 1961 were correlated in the work of the United Nations Scientific Committee on the Effects of Atomic Radiation [1].

Later Gibson [2], on the basis of systematic dose-rate measurements conducted from September, 1961, to August, 1962, at a height 1 m above ground level in the town of Groves, England, confirmed the presence of three clearly marked components of external background irradiation: cosmic rays, with an absorbed dose rate of 3.2 μrad/hour (26 mrad/year); natural radioactive isotopes contained in the soil, with a dose rate of 5.3 μrad/hour (46 mrad/year); and nuclear fallout, with a dose rate of 0.2 to 2 μrad/hour (depending on its "age").

Annual Doses of External Background Irradiation of Small Groups of Inhabitants of USSR Cities

City	Dosimeter exposure time, days	Value of background irradiation dose, mrad/year		
		minimum	maximum	average
Alma-Ata	263	90±22	140±32	110±18
Astrakhan	242	70±18	120±28	90±17
Askhabad	256	70±18	120±28	90±19
Baku	245	40±12	90±22	60±18
Vil'nyus	262	30±10	90±22	70±22
Vladivostok	237	80±20	120±28	100±14
Erevan	256	60±16	110±26	90±14
Irkutsk	281	90±22	150±34	120±22
Kiev	230	70±18	140±32	100±22
Kishinev	310	70±18	110±26	90±15
Leningrad	251	50±14	120±28	90±23
L'vov	227	70±18	140±32	110±21
Minsk	259	70±18	110±26	90±17
Murmansk	283	80±20	180±40	130±26
Novosibirsk	325	90±22	120±28	100±11
Orenburk	256	30±10	80±20	50±16
Petropavlovsk-Kamchatskii	227	70±18	100±24	90±13
Riga	201	90±22	130±30	110±17
Sevastopol'	167	30±10	70±18	40±12
Sochi	305	70±18	170±40	110±30
Tashkent	268	50±14	130±30	100±25
Tallin	201	80±20	150±34	110±22
Tbilisi	221	80±20	150±34	110±21
Khabarovsk	269	50±14	120±28	90±22
Chita	245	70±18	140±32	100±23
Yakutsk	264	40±12	110±26	70±21

In the United States, the dose rate of the external background irradiation in the vicinity of cities in Vermont and New Hampshire, measured with high-pressure ionization chambers and gamma spectrometers, was found to be 50-150 mrad/year [3].

According to the data of [4], the average dose rate of background irradiation, measured outdoors, above with granite deposits, was 104 mrad/year; above chalk deposits it was 31 mrad/year; and above clay deposits it was 61 mrad/year. The investigations used ionization chambers filled with nitrogen to a pressure of 50 atm. The measurements were made both indoors and outdoors. On the basis of these measurements and of approximate data on the average length of time spent by persons indoors and outdoors, the average annual doses of external irradiation per man were calculated. However, if we try to extrapolate the results of background irradiation dose-rate measurements conducted in various places where people may spend their time, so as to obtain the average tissue dose of irradiation of the people living in a given region, we may arrive at serious inaccuracies because of the indeterminacy in our estimates of the time spent by people indoors and outdoors.

In order to exclude such indeterminacies, the author of [5] proposed and used a portable individual dosi-

MOSCOW CONFERENCE OF COMECON SPECIALISTS ON APPLICATIONS FOR IONIZING RADIATIONS

V. P. Averkiev

Translated from Atomnaya Énergiya, Vol. 19, No. 3,
pp. 313-314, September, 1965

The Institute of Chemical Physics of the USSR Academy of Sciences was host to a conference of specialists from member nations of the Council for Mutual Economic Aid (COMECON] held in Moscow May 27-29, 1965,for the purpose of coordinating joint research projects on applications for high-level sources of ionizing radiations.

The conference heard two review reports by the USSR delegation, five by the Bulgarian, Polish, Roumanian, and Czech delegations, 18 original contributions on problems in radiation chemistry and radiobiology, and five papers by USSR delegates on radiation facilities.

Soviet scientists reported on the development of radiation processes which promise to be of substantial value to the national economy.

Of greatest interest for practical utilization was the method of radiation cross-linking of polyethylene initiated by special additives such as antioxidants and thermal stabilizers, so that the thermal resistance of polyethylene insulation material was improved by 50° to 100°C, the service life was stretched to 5000-6000 h at 150° and to 200 h at 200°C (ordinary polyethylene begins to "flow" at 100°).

Another focus of interest was the development of rubber radiation vulcanization technology, so that rubber can be produced without adding sulfur and rubber parts capable of withstanding heat loads to 410°C (the thermal stability of standard technical grade rubber is at most 100°C).

The following radiation processes were judged of potential industrial interest: grafting polymers from the vapor phase or liquid phase onto natural and synthetic fibers, glass fibers, or a mineral base; polymerization of fluoroolefins, telomerization of ethylene with carbon tetrachloride; modification of organic-impregnated wood materials, plywood, paper; synthesis of organotin compounds; sulfochlorination of synthine and polyethylene, oxidation of paraffins in the production of detergents; radiation-thermal cracking of petroleum to increase the yield of valuable unsaturated hydrocarbons.

Data were also reported on new approaches in the study of matter, including radiothermoluminescence, based on a comparison of the emission spectra of heated and pre-irradiated material and a reference spectrum, to gain information of fine structural changes in the test material.

Representatives of the Soviet Union attending the radiobiology panel gave an account of results of a study of pre-sowing irradiation of agricultural crop seeds. The investigation disclosed that ionizing radiation is a powerful tool in affecting the intensity and direction of exchange reactions in plant organisms, and the training of crops. Production tests confirmed the effectiveness of ionizing radiations. Pre-sowing exposures increased corn crops silage by 30%, cotton yield by 15 to 30%, potatoes by 20%, cabbage by 21%, carrots by 30%, radishes by 26%. The biochemical composition of root crops was improved at the same time, with increase in sugar, protein, and vitamin content.

Soviet scientists and designers also reported on the development of equipment for handling radiation processes under production conditions. Large isotope facilities with cobalt sources to 500 thousand gram-equivalents of radium have been built. Extensible indium-gallium loops for nuclear reactors, in up to 2 million gram-equivalents of radium, compact electron accelerators of 95% efficiency and up to 25 kW beam power accelerating electrons to 1.5 MeV energy, are now available, along with the portable seed irradiators GUPOS-800, GUPOS-GI, GUBE-800, GUBE-4000, and others.

Bulgarian scientists reported obtaining copolymers of polyformaldehyde with styrene, methylmethacrylate, propylene oxide. Products produced by the addition of various antioxidants and age resistors using radiation with no other stabilization measures were shown to exhibit enhanced thermal resistance.

SCIENTIFIC CONFERENCE OF THE MOSCOW ENGINEERING AND PHYSICS INSTITUTE [MIFI]

V. V. Frolov

Translated from Atomnaya Énergiya, Vol. 19, No. 3,
pp. 314-316, September, 1965

The annual Scientific Conference of the Moscow Engineering and Physics Institute, running from May 5 through May 21, 1965, scheduled 53 sessions and 22 panels, to hear a total of 210 papers. As in the preceeding year, the outstanding papers were presented by students as well as by faculty members.

Among the 2000 in attendance, 800 were representatives of research institutes, centers of higher learning, and industrial plants.

The panel on experimental nuclear physics showed greatest interest in a paper by V. V. Borog, V. G. Kirillov-Ugryumov and associates on the energy spectrum of cosmic muons at large zenith angles in the 10^{11} to 10^{12} eV energy range, in experiments using a 9 m^2 area ionization calorimeter. The preliminary measurements reported are in excellent accord with theory. V. D. Bobrov et al. reported experimental results of measurements of the rates of capture of negative muons by the nuclides $Ni^{51,60,62}$ and $Cr^{50,52,53,54}$. Comparison of experimental results and predictions based on the theory of finite Fermi systems showed a fit of absolute capture rates to within 10% and a relative variation in isotopic effect accurate to 3%. A paper by V. I. Gol'danskii and V. P. Shantorovich on the use of positronium in chemistry for research on the electronic structure of matter and on the kinetics of chemical reactions discussed some possible chemical research using muonium and positronium. A paper by V. I. Gol'danskii and I. P. Suzdalev demonstrated the effectiveness of the Mössbauer technique in studying thin surface oxide films, including those difficult to detect by other available methods, and established the mechanism in oxidation finely dispersed tin in air.

The theoretical nuclear physics panel heard an interesting paper by A. B. Migdal on recent results on the construction of a phenomenological approach to the theory of the nucleus as a many-body problem. The reporter and his students formulated gage invariance conditions and found the probabilities for single-particle transition in nuclei. Results of the application of this theory to quantitative calculations of muon capture cross sections in spherical nuclei were reported by G. G. Bunatyan. V. M. Novikov and M. G. Urin developed the qualitative theory of muon capture in a quasi-classical approximation valid for heavy nuclei. The audience responded with interest to A. S. Kompaneits and A. S. Chernov ("Solution of Cosmological Equations of Cylindrical Symmetry") obtaining solutions of Einstein's equations for a homogeneous axisymmetric model in two limiting cases: dustlike matter and an ultrarelativistic gas. Yu. A. Vdovin and V. M. Galitskii treated the kinetic equation for photons in a resonant medium. The investigation covered both a system of strictly resonant molecules and the spread of molecular energy levels. The way in which quantum effects influence multiple coulomb scattering of high-energy charged particles in matter was discussed in a paper by N. P. Kalashnikov and M. I. Ryazanov.

Six panels on experimental physics were held.

S. B. Shikhov and A. A. Ignatov described their procedure for calculating neutron relaxation length and asymptotic spectra in poor breeding media, a useful technique for treating constants of spherical harmonics. The paper by I. S. Slesarev and V. V. Khromov on new synthetic methods for calculating the space multidimensional distribution and space-angle distribution of neutron fields in reactors was found highly interesting. Using the method of arbitrary separation of variations, they reduced the initial equation with ease to a system of simple linear equations. The conference took note of the highly accurate results obtained calculating reactor systems by these methods, and the impressive savings in computer time. V. I. Davydov and S. B. Shikhov developed analytic methods for neutron field calculations. The use of matrix algebra enabled the authors to construct an efficient algorithm for use in calculations of multiregion nuclear reactors.

Some papers dealing with erosion of metal surfaces in low-pressure gas discharges triggered by ion beams and laser beams were submitted to the low-temperature plasma panel.

The panel on solid state physics showed peak interest in A. N. Oraevskii's report on chemical lasers, a report by Yu. A. Bykovskii and K. N. Vinogradov on double injection in silicon on a p-i-n structure, and a paper by R. K. Leonov and associates on a pulsed gas laser. The first of these papers cited voltage-current curves on silicon p-i-n structures having a negative resistance region, while the other reported pulsed laser action involving singly ionized argon.

There were also panels on automatic control and telemechanics, electronics, plasma physics, cybernetics, design of instruments and installations, strength and stress analysis and physics, etc.

Most of the papers presented are to be published by topics in scientific symposium issues edited by the MIFI.

INTERNATIONAL SYMPOSIUM ON NONDESTRUCTIVE TESTING IN NUCLEAR TECHNOLOGY

V. Gorskii

Translated from Atomnaya Énergiya, Vol. 19, No. 3, pp. 317-318, September, 1965

An international symposium on nondestructive testing of structural materials and components in nuclear industry was held in May 1965, in Bucharest, under IAEA auspices. This conference, the first of its kind, attracted 90-odd scientists from 19 countries. Forty-four papers were submitted. Representing the USSR were A. A. Kiselev, V. V. Gorskii, and V. G. Gerasimov.

In recent years, quality control of structural materials and of finished parts has been receiving exceptionally close attention. Methods used in nondestructive testing (ultrasonics, eddy currents, magnetic fields, x-rays, α-, β-, and γ-radiation, and miscellaneous techniques) have contributed in large measure to the improved strength and reliability in performance of parts and equipment. Nondestructive testing methods have won themselves a firm position in nuclear industry. This is explainable by the tighter requirements on service life of fuel elements and on strength of structural materials.

Representatives of all the leading nuclear centers and research laboratories in the USA (Los Alamos, Oak Ridge, Argonne, Savannah River, Hanford), Great Britain (Harwell, Warrington, Springfields), France (Saclay), Italy (Ispra), Belgium (Mol), and other countries presented papers to the conference, illustrating the state of techniques and methods in nondestructive testing of cladding materials for fuel elements, tubing for steam generators, reactor pressure vessels, completely fabricated fuel elements, welded joints, and techniques for monitoring the content and lengthwise distribution of uranium and plutonium in fuel elements, and similar related questions.

Inspection of Tubing

Tubing for fuel elements. An appreciable number of the papers submitted were devoted to quality control and measurement of the geometrical dimensions of thin-walled stainless steel tubing, zirconium alloys, aluminum alloys and SAP (sintered aluminum powder) for use in the fabrication of fuel element jackets. Ultrasonic inspection techniques (D. Worlton, USA; M. Destribat, France; F. Mann, Britain; W. Nyström, Sweden; and others) are in use predominantly to spot hidden flaws in tube walls (slag inclusions, cracks, oxide films, spalling) and to detect cracks and deep scratches on the inner and outer surfaces of tubes. Defects in tubing are detected by transverse waves and Lamb waves. The pulsed echo method for inspection in water is common: operating frequencies range from 2 to 15 MeV. Two sets of ultrasonic wave receivers and transmitters are placed crosswise and lengthwise to the tube axis to detect flaws. Inspection proceeds at a rate of 0.3 to 0.5 meter per minute. All delegates to the symposium were interested in defect size allowances in tubes and fuel element jackets. Direct data on the degree of hazard involved in defects of specified dimensions in fuel element jackets are not available from results of in-pile tests, but there are plans for performing tests of this nature (Belgium, P. Libbotte). In analyzing all the contributions at the symposium, we may state that suitable criteria for scrapping zirconium alloy tubes would be scratches to 5% of the tube wall thickness and extending several millimeters (to 10 mm in fact) in length, or 10% of wall thickness for stainless steel tubing.

Eddy current methods in quality control of tubing are in less frequent use, since the method is less sensitive in the view of some reporters. But K. Rencken (USA) feels that stainless steel tubing of less than 6 mm diameter and less than 0.75 mm wall thickness should be inspected by pulsed eddy currents. The sensitivity to fine-scale defects is the same as for ultrasonic methods, and the inspection proceeds at a rate several times faster (tubes 9.55 by 0.5 mm have been inspected at a rate of 4 meters/min). This view is sustained by F. Förster and T. Müller (West Germany).

The wall thickness of smooth tubes and finned tubes with fins spaced greater than 2 mm is measured by an ultrasonic water-immersion resonance method (F. Wells, R. Sharpe, Britain; A. Van der Linde, Netherlands; S. Lund,

Inspection of reactor pressure vessels was discussed by W. McGonnagle, G. Tenney (USA), R. Filip (Chechoslovakia), and D. Horvat (Yugoslovia). Methods for monitoring U^{235} content and distribution (A. McEachern, Canada), Pu^{242} content, using isotope dilution techniques (G. Chenoir, France), boron content (W. Francis, USA), the structure of sintered materials (E. Labusca, Rumania), and miscellaneous topics were also discussed.

The range of application of nondestructive testing techniques are continually expanding. The use of infrared radiation, microwave techniques, x-ray television systems employing vidicons sensitive to the x-ray wavelengths, are among the most promising developmental techniques. Nondestructive techniques are being used not only in flaw detection, but also to determine the physical contents of materials.

The symposium was very well organized, proceeded in a businesslike atmosphere, and contributed to a liberal exchange of views on current topics and avenues of development of NDT.

The proceedings of the NDR symposium will be published by IAEA in late 1965.

of cosmic particles of greater than 10^{11} eV energy that such cases can be understood by assuming the existence of a particle with a geometric interaction cross section 1/30 the geometric cross section of the nucleus, a lifetime longer than $3 \cdot 10^{-7}$ sec, and mass approximately $10m_p$.

If unitary symmetries make it possible to classify strongly interacting particles and to sometimes predict their masses and properties, then another direction the theory of strongly interacting particles could take would be probing into the asymptotic properties of scattering amplitudes. Restrictions on the asymptotic behavior of the amplitudes based on analyticity and unitarity were discussed in the lecture by A. Marten (CERN), K. A. Ter-Marticosyan discussed the Regge pole model in the light of new experimental data. New experimental findings were discussed in lectures by L. N. Strunov, "Experimental studies of nuclear amplitudes of forward scattering processes at high energies," A. L. Lyibimov, "Particle scattering at high energies at high momentum transfer," and F. Duke (Britain), "Data on π-p-scattering at 1 GeV." New data on pion charge transfer and on pion scattering by nucleons (backward scattering) were reported by V. A. Shebanov and Yu. V. Galaktionov.

The topic "Weak interactions and parity violation" was the subject of lectures by I. Yu. Kobzarev on the properties of vectorial constants in strange decays, by M. Schwartz (USA) on neutrino physics and searches for the intermediate boson, by V. S. Evseev on the coupling constant in μ-capture, by P. A. Krupchitskii on the existence of an internucleon potential breaking space parity, etc.

Of greatest interest was the lecture by L. B. Okun' reporting new work by Lee, Bernstein, and Feynmann on possible nonconservation of C-parity in electromagnetic interactions. This far-reaching suggestion advanced to account for the famour Cronin effect (the decay $K_2^0 \rightarrow \pi + \pi$) may be varified in a series of independent experiments. It is essential, though, that nonconservation of C-parity is not manifested in the generally observable elastic coulomb scattering processes. But the asymmetry of π^+- and π^--mesons in the Dalitz diagram for the electromagnetic decay $\eta \rightarrow 3\pi$ is to be expected. The total worldwide statistics on this mode of decay seem to indicate some such asymmetry, despite the low reliability of the data. Ther are at present no experimental facts to contradict the hypothesis.

Lectures on electromagnetic interactions may be grouped under two headins. K. Strauch, V. Fisher, and I. Pless (USA) spoke on photoproduction of particles, isobars, and meson resonances at high energies. L. Lederman discussed in some detail the present status of a wide variety of experiments designed to check the range of applicability of electrodynamics. He also gave an account on experiments on proton scattering of muons and compared these data to findings in electron-proton scattering.

Four reports dealt with experimental techniques. I. Pless and F. Solmitz addressed the school on automatic scanning, data processing, and data analysis for handling bubble chamber and spark chamber results. In his lecture "Spark chambers," K. Strauch centered his attention on the properties of chambers with large interelectrode spacing and discharge track delineation. We note that spark chambers with large discharge gap have been studied most intensively in the Soviet Union and are now awakening great interest in the USA. A. I. Alikhanyan dwelt on new techniques in the detection of high-energy particles. He cited new data on the properties of track delineation chambers and projection spark chambers, supplementing the lecture by E. Strauch, told of original attempts to measure particle energy by recording radiation emitted in transitions and by measuring ionization losses in layered emitters, and made public the results of the first experiments.

This article cannot mention all the lectures, still less provide a full and detailed account of their contents. Some of the latest results of greatest interest were only sketched. Once again we stress that this was a school, not a conference, and the lectures dealt for the most part with relatively known results. Some topics were discussed in detail at the seminars devoted to symmetries, to processing experimental data, to spark chambers. Scientific contacts outside the lectures were most fruitful.

In conclusion, expressing the view of those in attendance, we should like to thank the organizers, and in particular A. I. Alikhanyan whose efforts contributed mightily to the successful outcome.

All the proceedings of the session will be published by the Academy of Sciences of the Armenian SSR.

IAEA CONFERENCE ON PERMISSIBLE EXPOSURE DOSAGE

Translated from Atomnaya Énergiya, Vol. 19, No. 3,
p. 320, September, 1965

A conference of experts on protection of the population from radiation accidents met in Vienna in May 1965. This was the third such Vienna conference under joint sponsorship of IAEA and the World Heath Organization, to develop recommendations for protection of the population from radiation hazard in the event of catastrophic accidents at nuclear facilities.

Representatives of 14 member nations of IAEA and of 6 international bodies met to discuss a plan of recommendations drawn up by the preceding conference. This plan was found to be too narrow to encompass all related problems (e.g., there are no data on regularities governing the migration of radioisotopes according to biological chains, etc.). The force of the recommendations was restricted to cases of major accidents where large sections of the population might become exposed to radiation, and the doses exceed those specified in the basic rules for protection from exposure.

The document drawn up consists of two major parts. The first rates the probability of occurrence of leukemias, thyroid and bone tumors and neoplasms in other tissues, and the genetic sequelae of radiation exposure depending on absorbed dose and other factors. The second major part presents the principles for calculating tissue doses and buildup of levels of radioisotopes (I^{131}, Sr^{90}, etc.) and materials on the biological effects of radiation exposure.

The experts approved a suggestion from IAEA to set a dose of 25 rad in assessing the safety of large nuclear installations, thereby indicating that the size of permissible doses for that estimate may exceed the exposure levels of the population accepted by the International Commission on Radiation Shielding and by IAEA by as much as 1 to 100 times depending on the concrete conditions (the levels mentioned are included in the basic radiation safety standards).

SOVIET JOURNALS AVAILABLE IN COVER-TO-COVER TRANSLATION

This list includes all Russian journals which—to the publisher's knowledge—were available in cover-to-cover translation on June 30, 1965, or for which definite and immediate plans for cover-to-cover translation had been announced by that date. The list reflects only *current* publication arrangements, but the date and issue listed for first publication refer to translations available from any source. Thus, earlier volumes of a translation journal may have been published by an organization other than that listed as the current publisher, and possibly under a different title (and, for *Doklady Akademii Nauk SSSR*, in a different arrangement of sections).

Five bits of information are furnished, separated by bullets:

1. The abbreviation(s) by which the journals are most frequently referred to in Russian bibliographies (if the name of the journal is customarily spelled out, no abbreviation is given).
2. The transliterated full name of the journal.
3. The full name of the translation journal (in bold type).
4. The year, volume (in parentheses), and issue of first publication of the translation (parentheses are empty if the Russian journal does not use volume numbers).
5. The current publisher of the translation [AGI—American Geological Institute, AGU—American Geophysical Union, AIP—American Institute of Physics, CB—Consultants Bureau, CH—Clearing House for Federal Scientific and Technical Information, CS—The Chemical Society (London), FP—Faraday Press, IEEE—Institute of Electrical and Electronic Engineers, ISA—Instrument Society of America, PP—Pergamon Press].

For convenience in locating bibliographic references the journals are listed in alphabetical order of the *abbreviated* titles.

AÉ • Atomnaya énergiya • **Soviet Journal of Atomic Energy** • 1956(1)1 • CB

Akust. zh. • Akusticheskii zhurnal • **Soviet Physics—Acoustics** • 1955(1)1 • AIP

Astrofiz. • Astrofizika • **Astrophysics** • 1965(1)1 • FP

Astr(on). zh(urn). • Astronomicheskii zhurnal • **Soviet Astronomy—AJ** • 1957(34)1 • AIP

Avtomat. i telemekh. • Avtomatika i telemekhanika • **Automation and Remote Control** • 1956(27)1 • ISA

Avto(mat). svarka • Avtomaticheskaya svarka • **Automatic Welding** • 1959(12)1 • British Welding Research Association

Avtometriya • **Autometry** • 1965(1)1 • CB

Biokhim. • Biokhimiya • **Biochemistry** • 1956(21)1 • CB

Byul. éksp(erim). biol. (i med.) • Byulleten' éksperimental'noi biologii i meditsiny • **Bulletin of Experimental Biology and Medicine** • 1959(41)1 • CB

DAN (SSSR) • *see* Doklady AN SSSR

Defektoskopiya • **Soviet Defectoscopy** • 1965(1)1 • CB

Diff. urav. • Differentsial'nye uravneniya • **Differential Equations** • 1965(1)1 • FP

Dokl(ady) AN SSSR; DAN (SSSR) • Doklady Akademii Nauk SSSR • The translation of Doklady is published in various journals, according to subject matter. The sections of Doklady contained in each of the translation journals are listed in parentheses.

Doklady Biochemistry (biochemistry) • 1957(112)1 • CB

Doklady Biological Sciences Sections (anatomy, cytology, ecology, embryology, endocrinology, evolutionary morphology, parasitology, physiology, zoology) • 1957(112)1 • CB

Doklady Biophysics (biophysics) • 1957(112)1 • CB

Doklady Botany (botany, phytopathology, plant anatomy, plant ecology, plant embryology, plant physiology, plant morphology) • 1957(112)1 • CB

Doklady Chemical Technology (chemical technology) • 1956(106)1 • CB

Doklady Chemistry (chemistry) • 1956(106)1 • CB

Doklady Earth Sciences Sections (geochemistry, geology, geophysics, hydrogeology, lithology, mineralogy, paleontology, permafrost, petrography) • 1959(124)1 • AGI

Doklady Physical Chemistry (physical chemistry) • 1957(112)1 • CB

Doklady Soil Science (soil science) • 1964(154)1 • Soil Science Society of America

Soviet Mathematics—Doklady (mathematics) • 1960(130)1 • American Mathematical Society

Soviet Oceanography (oceanology) • 1959(124)1 • AGU

Soviet Physics—Doklady (aerodynamics, astronomy, crystallography, cybernetics and control theory, electrical engineering, energetics, fluid mechanics, heat engineering, hydraulics, mathematical physics, mechanics, physics, technical physics, theory of elasticity • 1956(106)1 • AIP

Élektrokhimiya • **Soviet Electrochemistry** • 1965(1)1 • CB

Élektrosvyaz' • combined with Radiotekhnika in **Telecommunications and Radio Engineering** • 1957(16)1 • IEEE

Élektrotekh. • Élektrotekhnika • **Soviet Electrical Engineering** • 1965(36)1 • FP

Éntom(ol). oboz(r). • Éntomologicheskoe obozrenie • **Entomological Review** • 1958(37)1 • Entomological Society of America

Fiz. goreniya i vzryva • Fizika goreniya i vzryva • **Combustion, Explosion, and Shock Waves** • 1965(1) • FP

Fiziol(ogiya) rast. • Fiziologiya rastenii • **Soviet Plant Physiology** • 1957(4)1 • CB

Fiz.-khim. mekh(anika) mater(ialov); FKhMM • Fizikokhimicheskaya mekhanika materialov • **Soviet Materials Science** • 1965(1)1 • FP

Fiz. met. i metallov.; FMM • Fizika metallov i metallovedenie • **Physics of Metals and Metallography** • 1957(5)1 • Acta Metallurgica

Fiz.-tekhn. probl. razr. polezn. iskopaem. • Fizikotekhnicheskie problemy razrabotki poleznykh iskopaemykh • **Soviet Mining Science** • 1965(1)1 • CB

Fiz. tv(erd). tela; FTT • Fizika tverdogo tela • **Soviet Physics—Solid State** • 1959(1)1 • AIP

FKhMM • *see* Fiz.-khim. mekhanika materialov

FMM • *see* Fiz. met. i metallov.

FTT • *see* Fiz. tverd. tela

Geliotekh. • Geliotekhnika • **Applied Solar Energy** • 1965(1)1 • FP

Geol. nefti i gaza • Geologiya nefti i gaza • **Petroleum Geology** • 1958(2)1 • Petroleum Geology, Box 171, McLean, Va.

Geomagnet. i aéronom. • Geomagnetizm i aéronomiya • **Geomagnetism and Aeronomy** • 1961(1)1 • AGU

Inzh.-fiz. zh. • Inzhenerno-fizicheskii zhurnal • **Journal of Engineering Physics** • 1965(8)1 • FP

Inzh. zh. • Inzhenernyi zhurnal • **Soviet Engineering Journal** • 1965(5)1 • FP

Iskusstv. sputniki Zemli • Iskusstvennye sputniki Zemli • **Artificial Earth Satellites** • 1958(1)1 • CB [superseded by Kosmich. issled.]

Izmerit. tekhn(ika) • Izmeritel'naya tekhnika • **Measurement Techniques** • 1958(7)1 • ISA

Izv. AN SSSR, o(td.) kh(im.) n(auk) (*or* ser. khim.) • Izvestiya Akademii Nauk SSSR: Otdelenie khimicheskikh nauk (*or* Seriya khimicheskaya) • **Bulletin of the Academy of Sciences of the USSR: Division of Chemical Science** • 1952(16)1 • CB

Izv. AN SSSR, ser. fiz(ich). • Izvestiya Akademii Nauk SSSR: Seriya fizicheskaya • **Bulletin of the Academy of Sciences of the USSR: Physical Series** • 1954(18)3 • Columbia Technical Translations

Izv. AN SSSR, ser. fiz. atm. i okeana • Izvestiya Akademii Nauk SSSR: Seriya fiziki atmosfery i okeana • **Izvestiya, Atmospheric and Oceanic Physics** • 1965( )1 • AGU

Izv. AN SSSR, ser. fiz. zemli • Izvestiya Akademii Nauk SSSR: Seriya fiziki zemli • **Izvestiya, Physics of the Solid Earth** • 1965( )1 • AGU

Izv. AN SSSR, ser. geofiz. • Izvestiya Akademii Nauk SSSR: Seriya geofizicheskaya • **Bulletin of the Academy of Sciences of the USSR: Geophysics Series** • 1957(7)1 • AGU [superseded by Izv. AN SSSR, ser. fiz. atm. i okeana and Izv. AN SSSR, ser. fiz. zemli]

Izv. AN SSSR, ser. geol. • Izvestiya Akademii Nauk SSSR: Seriya geologicheskaya • **Bulletin of the Academy of Sciences of the USSR: Geologic Series** • 1958(23)1 • AGI

Izv. AN SSSR, ser. neorgan. mat(er). • Izvestiya Akademii Nauk SSSR: Seriya neorganicheskie materialy • **Inorganic Materials** • 1965(1)1 • CB